angle, θ_R, were calculated. The mobility factor (M_f) was calculated using the following equation to evaluate the mobility of the polymer chains at the surface [9]:

$$M_f = (\theta_A - \theta_R)/\theta_A.$$

Wettability by water was also evaluated by an immersion method with an aqueous solution containing water-soluble dye (Crystal violet). The PE and PE/PMPC alloy membranes were immersed in the solution and maintained for 10 s, then lifted up and observed visibly.

The scanning electron microscope (SEM, SEM-5400, JEOL, Tokyo, Japan) was used for observation of the polymer alloy membranes. The tensile strength of the membranes was measured using an autograph (Strograph V10-C, Toyo-seiki, Tokyo, Japan) at a 0.2 mm/min crosshead speed.

2.4. Evaluation of platelet adhesion on the polymer membrane

Human platelet-rich plasma (PRP) was prepared from citrated whole blood by centrifugation at 1200 rpm for 15 min. A round PE/PMPC alloy membrane (15 mm in diameter) was prepared, and the membrane was then placed in a 24-well culture plate using the same procedure as previously reported. To equilibrate the membrane, PBS was added to each well and allowed to remain for 15 h. After removing the PBS, 0.7 ml of PRP was poured onto the membrane and allowed to remain at 37°C for 3 h. The PRP was then removed with an aspirator, and the membrane was rinsed three times with PBS. One milliliter of 2.5 wt% glutaraldehyde in PBS was then poured into each well and kept for 2 h to fix the adhered platelets. After removing the glutaraldehyde solution, the membrane was rinsed five times with pure water. The membrane was freeze-dried and coated with gold to examine the surface by SEM. More than three membranes were examined, and representative SEM pictures are shown.

3. Results and discussion

3.1. Formation of polymer alloy composed of PE and PMPC

In our previous reports, we demonstrated that the biocompatibility of conventional polymers used for the preparation of medical devices, such as SPU [2,3], PSf [4,5] cellulose acetate (CA) [6] and poly(lactic acid) (PLA) [7], is improved by blending with MPC polymers. The molecular structure of the MPC polymer was controlled to adjust the solubility in the matrix polymer. For example, when the MPC polymer was blended into SPU, we prepared poly(MPC-*co*-2-methacryloyloxyethyl butylurethane), which possesses a urethane bond in the side chain [10,11]. Because the urethane bond is expected to have affinity for SPU and solvents of SPU such as *N*,*N*-dimethylformamide (DMF), this MPC polymer shows good compatibility with SPU. On the other hand, in the case of PE, there is no way to design the molecular structure of the MPC polymer to achieve compatibility with PE. PE is a simple hydrocarbon polymer; therefore, it is inert to other chemical compounds except for hot xylene. Moreover, the crystalline structure of PE is stable. At first, we synthesized a series of MPC polymers having a long hydrocarbon chain in the side chain [12]. However, poly(MPC-*co*-stearyl methacrylate) and poly(MPC-*co*-dodecyl methacrylate) could not be blended in PE well. PMPC is a water-soluble hydrophilic polymer, and due to the bulky phosphorylcholine group in the side chain, it assumes a compact configuration. We hypothesized that the PMPC is a suitable MPC polymer for blending in PE due to this compact configuration, because when the PMPC is inserted into the PE matrix, it can remain between the crystalline regions of PE. Thus, we tried to form a polymer alloy composed of PE and PMPC. By using solution mixing and evaporation (see Fig. 2), we could obtain a PE/PMPC alloy membrane having various PMPC compositions from 0 to 15 wt%. A light opaque membrane was obtained when the PMPC composition was 10 wt%. We used the PE/PMPC alloy membrane whose PMPC content was 10 wt% for the following evaluation of surface and bulk properties.

Fig. 3 shows SEM pictures of the PE/PMPC alloy membrane during the membrane forming process with solvent evaporation. The PMPC domains were stained with RuO_4 and they are observed as the much darker part compared with the PE matrix. Just after the polymer mixture solution was poured onto the substrate and cooled to room temperature, the PE formed a small crystalline matrix. Accompanying the evaporation of BuOH, which is a good solvent for PMPC and has a lower boiling temperature than that of xylene, the PMPC chains began to aggregate and formed domains (Fig. 3A and B) which were located at the surface and could be observed well. When xylene began to evaporate, the PE chains dissolved in xylene were then precipitated and covered the PMPC domains at the surface (Fig. 3C). Finally, the polymer alloy membrane composed of PE and PMPC was obtained by complete removal of these solvents by vacuum drying (Fig. 3D). According to the SEM picture, Fig. 3D, PMPC domains still were observed at the surface.

Since the PMPC is a water-soluble polymer, there is a possibility of detaching the PMPC from the PE/PMPC alloy membrane on immersion in water. We tried to determine the amount of PMPC in aqueous medium after immersion of a PE/PMPC alloy membrane in water at 30°C for 1 week. However, no PMPC could be

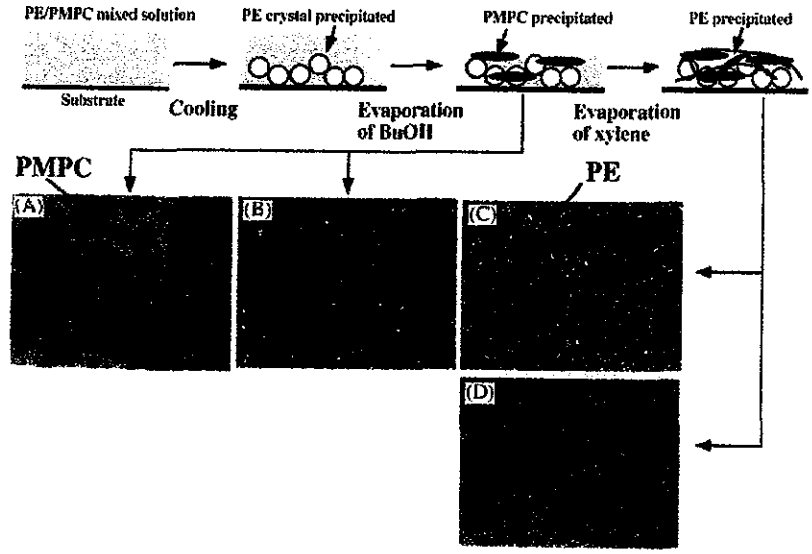

Fig. 3. SEM pictures of PE/PMPC alloy membrane during the membrane-forming process.

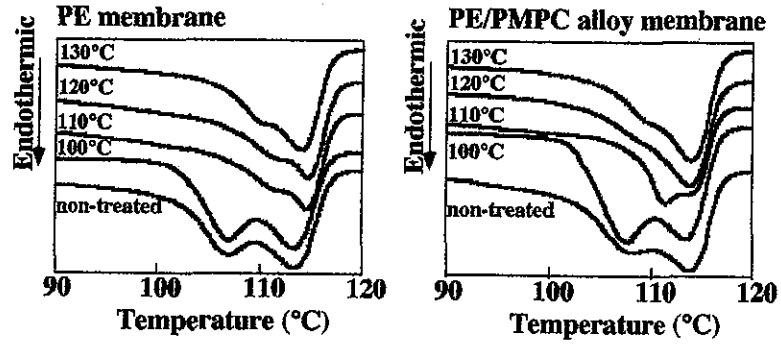

Fig. 4. DSC curves of PE and PE/PMPC alloy membranes after thermal treatment.

detected. It is considered that the PMPC chains were entangled the with PE chains and were immobilized completely during alloy formation.

Fig. 4 shows typical DSC curves of PE and PE/PMPC alloy membranes after thermal treatment at a given temperature. Both the PE and PE/PMPC alloy membranes without thermal treatment had two endothermic peaks at 107°C and 114°C. The higher peak temperature corresponded to the melting point of the crystalline portion of PE. After applying the thermal treatment, the lower peak temperature shifted towards the high temperature region. The relationship between the lower peak temperature and the thermal treatment temperature is indicated in Fig. 5. In the case of the PE membrane, the lower peak temperature began to shift when the PE membrane was annealed at 115°C, that is, above the melting temperature. The addition of PMPC induced a lowering of the temperature, and the lower peak temperature began to shift on the DSC curve. The lower peak temperature corresponded to melting of the

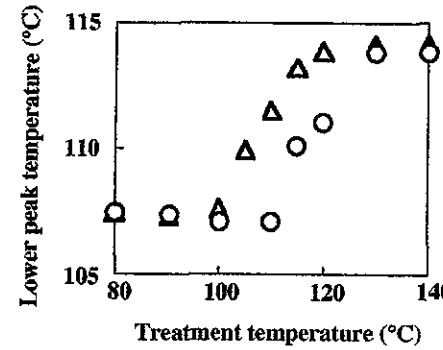

Fig. 5. Relationship between lower peak temperature and thermal treatment temperature: circle, PE membrane; triangle, PE/PMPC alloy membrane.

semi-crystalline region, which was formed by the precipitated PE chains during the solvent evaporation process. That is, the PMPC chains affected the semi-crystalline structure of PE. By applying the thermal

treatment at 120°C, the lower peak was substantially diminished. This is due to the semi-crystalline domain of PE being converted to a much higher crystalline state. From these results, we selected two temperatures, such as 80°C and 120°C, as the thermal treatment temperature and investigated the surface and bulk properties of the PE/PMPC alloy membrane.

3.2. Surface characteristics of the PE/PMPC alloy membrane

In Fig. 6, the XPS charts of PE and PE/PMPC alloy membranes are displayed. In the case of the PE membrane, a carbon signal at 285 eV was observed but no signal was found in the oxygen, nitrogen and phosphorus regions. On the other hand, signals attributed to carbon, oxygen, nitrogen, and phosphorus were observed for the PE/PMPC alloy membrane without thermal treatment. That is, the phosphorylcholine groups in the MPC unit were located at the surface. After thermal treatment at 80°C, the intensity of the phosphorus signal decreased but every signal corresponding to the phosphorylcholine group was observed. Even when the PE/PMPC alloy membrane was annealed at 120°C, the phosphorylcholine group still remained on the surface. Moreover, the carbon signal at 288 eV, which is attributed to the ester linkage of the MPC unit, appeared clearly. Therefore, migration of both polymer chains was occurring during thermal treatment above the melting temperature of the PE crystal. SEM observation of the surface and cross-section of the PE/PMPC alloy membrane also supported the results of the XPS measurement. Before the thermal treatment, many PMPC domains are observed at the surface as bright regions in Fig. 7(A). Thermal treatment at 80°C decreased in the number of PMPC domains. After thermal treatment at 120°C, the surface of the PE/PMPC alloy membrane had a uniform surface. By combination with the XPS result, the PMPC chains existed but they were homogeneously located at the surface. Because the MPC units are hydrophilic, the wettability by water of the surface of the PE became greater on introduction of PMPC. Fig. 8 shows a picture of the PE and PE/PMPC alloy membranes after immersion in aqueous solution containing a water-soluble dye. In these pictures, a dark colored part represents the dye solution remained on the surface even when the polymer membranes pulled up from the solution. On the surface of the PE membrane, the dye solution was repelled. Wettability was improved in the case of the PE/PMPC alloy membrane even after thermal treatment at 120°C. We also carried out a DCA measurement and evaluated the mobility of the functional group at the surface when the polymer membrane contacted water, that is, the polymer surface changed from the dry state to the wet state. The mobility factor is a suitable parameter for evaluating the surface mobility [9]. In Fig. 9, the mobility factors of PE and PE/PMPC alloy membrane are summarized. The values of the PE and PE/PMPC alloy membranes without thermal treatment were 0.092 and 0.25, respectively. This clearly showed that the surface mobility of PE/PMPC alloy membrane was higher than that of PE. This is due to the PMPC in the polymer alloy. Applying the thermal treatment to the PE/PMPC alloy membrane induced reduction of the mobility factor. That is, the PE matrix immobilized the PMPC chains more tightly. However, even after thermal treatment at 120°C, the

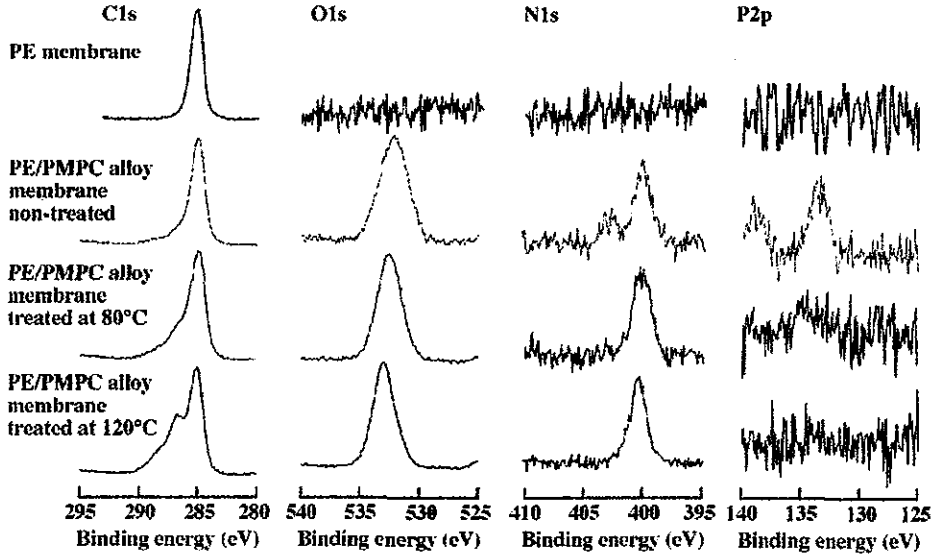

Fig. 6. XPS chart of PE and PE/PMPC alloy membranes.

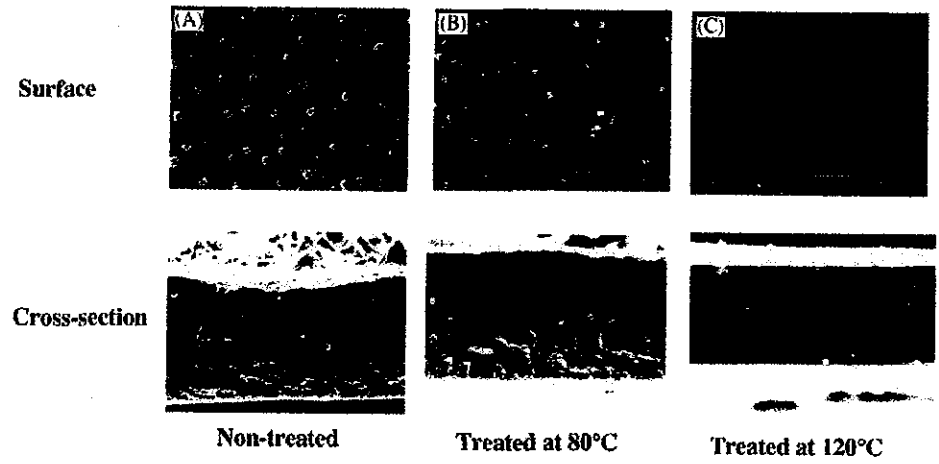

Fig. 7. SEM pictures of PE/PMPC alloy membrane after thermal treatment: (A) non-treated, (B) thermally treated at 80°C, (C) thermally treated at 120°C.

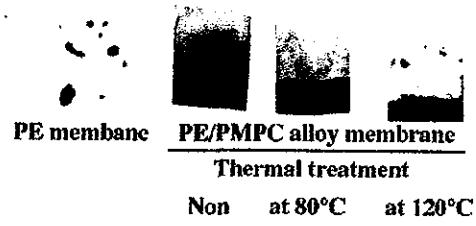

Fig. 8. Picture of PE and PE/PMPC alloy membranes after immersion into aqueous solution containing water-soluble dye.

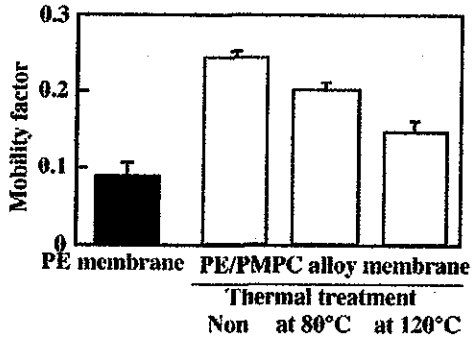

Fig. 9. Mobility factor of PE and PE/PMPC alloy membranes.

mobility factor became greater compared with that of PE. These surface analyses revealed that the PMPC chains appeared on blending with PE just after the PE/PMPC alloy membrane was prepared by solution mixing and solvent evaporation, Thermal treatment at lower temperature maintained the surface properties at almost the same level as that without thermal treatment. Though thermal treatment at a higher temperature induced coverage of the PE matrix at the surface, the effect of PMPC on the surface properties was remained.

3.3. Mechanical properties of the PE/PMPC alloy membrane

Mechanical strength measurement was carried out to evaluate the bulk properties of the PE/PMPC alloy membrane. Fig. 10 shows various mechanical properties of the PE and PE/PMPC alloy membranes. By comparison with the PE membrane, tensile strength and breaking elongation of the PE/PMPC alloy membrane were lower. However, these were recovered by thermal treatment. On the other hand, Young's modulus of the PE membrane slightly increased on blending with PMPC. Thermal treatment enhanced this tendency. The PMPC chains strongly affected the bulk structure of PE. The mechanical properties of PE depend on the crystalline content and size in the matrix. During membrane processing, small-sized PE crystals were formed before blending of PMPC and semi-crystalline PE and amorphous PMPC was precipitated. That is, the PMPC chains disturbed the connection of the PE crystals. By applying a thermal treatment, the PE crystals were connected with each other. In particular, when the PE/PMPC alloy membrane was annealed at 120°C, which is above the melting temperature of PE, the connection among PE crystals proceeded well.

3.4. Platelet adhesion on the PE/PMPC alloy membrane

Platelet adhesion on the PE and PE/PMPC alloy membranes was evaluated. Fig. 11 shows that SEM pictures of those membranes after contact with a platelet suspension. On the surface of the PE membrane, many platelets adhered and were deformed significantly. On the other hand, few platelets adhered on the PE/PMPC alloy membrane. It is well-known that the MPC polymer shows excellent blood compatibility [13–18]. Thus, the

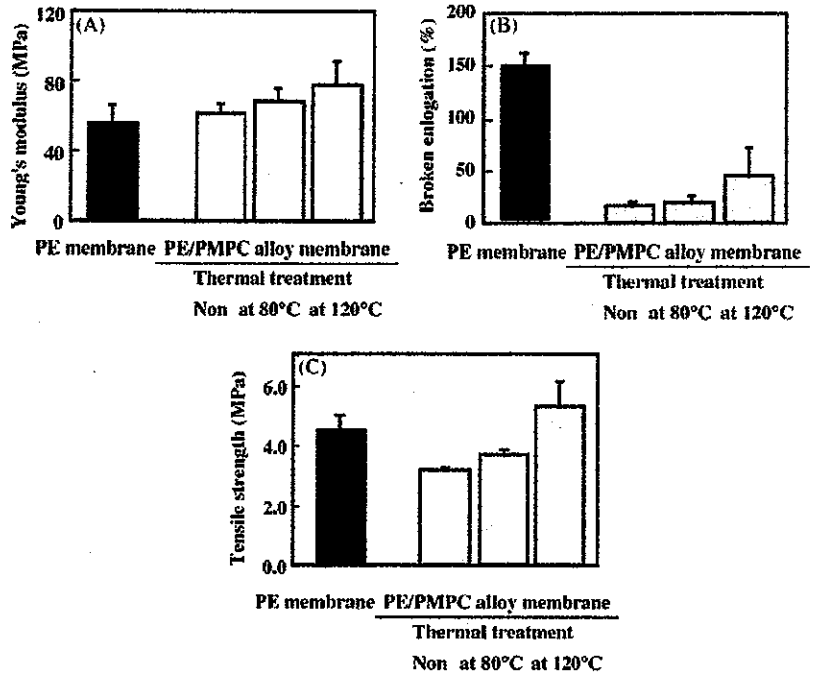

Fig. 10. Mechanical properties of PE and PE/PMPC alloy membranes: (A) Young's modulus, (B) broken elongation, (C) tensile strength.

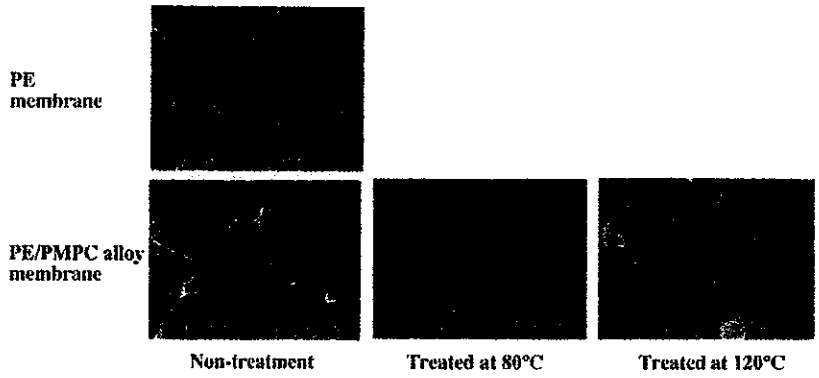

Fig. 11. Platelet adhesion on PE and PE/PMPC alloy membranes.

PMPC in the PE matrix of the polymer alloy played a significant role in reducing platelet adhesion.

4. Conclusion

We successfully prepared a polymer alloy composed of apolar PE and a hydrophilic phospholipid polymer, PMPC. PMPC domains were located at the surface even after the solvent was completely evaporated, and they altered the surface properties significantly compared with those of PE. Thermal treatment was applied to improve the mechanical properties above and below the melting temperature of PE matrix. Adhesion of platelets on the surface of PE/PMPC alloy membrane was suppressed compared with that on original polyethylene membrane. The PE/PMPC alloy is a promising material as an alternative to PVC.

Acknowledgements

A part of this study is supported by JSPS (13480288) and by a Grant for 21st Century COE Program "Human-Friendly Materials based on Chemistry" from the Ministry of Education, Culture, Sports, Science, and Technology of Japan.

References

[1] Wang A, Essner A, Klein R. Abstract effect of contact stress on friction and wear of ultra-high molecular weight polyethylene in total hip replacement. Proc Inst Mech Eng [H] 2001;215:133–9.

[2] Ishihara K, Shibata N, Tanaka S, Iwasaki Y, Kurosaki T, Nakabayashi N. Improved blood compatibility of segmented polyurethane by polymeric additives having phospholipid polar group 2. Dispersion state of polymeric additive and protein adsorption on the surface. J Biomed Mater Res 1996; 32:401–8.

[3] Yoneyama T, Ishihara K, Nakabayashi N, Ito M, Mishima M. Short-term in vivo evaluation of small-diameter vascular prosthesis composed of segmented polyurethane/2-methacryloyloxyethyl phosphorylcholine polymer blend. J Biomed Mater Res Appl Biomater 1998;41:15–20.

[4] Ishihara K, Fukumoto K, Iwasaki Y, Nakabayashi N. Modification of polysulfone with phospholipids polymer for improvement of blood compatibility. Part 1. Surface characterization. Biomater 1999;20:1545–51.

[5] Hasegawa T, Iwasaki Y, Ishihara K. Preparation of blood-compatible hollow fibers from a polymer alloy composed of polysulfone and 2-methacryloyloxyethyl phosphorylcholine polymer. J Biomed Mater Res Appl Biomater 2002;63:333–41.

[6] Ye S-H, Watanabe J, Iwasaki Y, Ishihara K. Novel cellulose acetate membrane blended with phospholipids polymer for hemocompatible filtration system. J Membr Sci 2002;210: 411–21.

[7] Iwasaki Y, Sawada S, Ishihara K, Khang G, Lee H-B. Reduction of surface-induced inflammatory reaction on PLGA/MPC polymer blend. Biomaterials 2002;23:3897–903.

[8] Ishihara K, Ueda T, Nakabayashi N. Preparation of phospholipid polymers and their properties as hydrogel membrane. Polym J 1990;23:355–60.

[9] Kataoka K, Taira H, Kikuchi A, Tsuruta T, Hayashi H. In: Akutsu T, Koyanagi H, editors. Heart replacement—artificial heart, vol. 5. Tokyo: Springer; 1996. p. 29.

[10] Ishihara K, Hanyuda H, Nakabayashi N. Synthesis of phospholipid polymers having a urethane bond in the side chain as coating material on segmented polyurethane and their platelet adhesion-resistant properties. Biomaterials 1995;16:873–9.

[11] Ishihara K, Iwasaki Y. Biocompatible elastomers composed of segmented polyurethane and 2-methacryloyloxyethyl phosphorylcholine polymer. Polym Adv Technol 2000;11:626–34.

[12] Ueda T, Oshida H, Kurita K, Ishihara K, Nakabayashi N. Preparation of 2-methacryloyloxyethyl phosphorylcholine copolymers with alkyl methacrylates and their blood compatibility. Polym J 1992;24:1259–69.

[13] Ishihara K, Aragaki R, Ueda T, Watanabe A, Nakabayashi N. Reduced thrombogenicity of polymers having phospholipid polar group. J Biomed Mater Res 1990;24:1069–77.

[14] Ishihara K, Oshida H, Ueda T, Endo Y, Watanabe A, Nakabayashi N. Hemocompatibility of human whole blood on polymers with a phospholipid polar group and its mechanism. J Biomed Mater Res 1992;26:1543–52.

[15] Ishihara K, Ziats NP, Tierney BP, Nakabayashi N, Anderson JM. Protein adsorption from human plasma is reduced on phospholipid polymer. J Biomed Mater Res 1991;25:1397–407.

[16] Campbell EJ, Byrne VO, Stratford PW, Quirk I, Vick TA, Wiles MC, Yianni YP. Biocompatible surface using methacryloylphosphoryl-choline laurylmethacrylate copolymer. ASAIO J 1994;40:853–7.

[17] Zhang S, Benmarkroha Y, Rolf P. Blood-compatible materials based on cell membrane mimicry for intravascular sensors. Celler Eng 1996;1:103–8.

[18] Sugiyama K, Aoki H. Surface modified polymer microspheres obtained by the emulsion copolymerization of 2-methacryloyloxyethyl phosphorylcholine with various vinyl monomers. Polym J 1994;26:561–9.

JOURNAL OF BONE AND MINERAL RESEARCH
Volume 19, Number 7, 2004
Published online on May 24, 2004; doi: 10.1359/JBMR.040513

Osteoclast Differentiation by RANKL Requires NF-κB–Mediated Downregulation of Cyclin-Dependent Kinase 6 (Cdk6)

Toru Ogasawara,[1] Mika Katagiri,[1] Aiichiro Yamamoto,[1] Kazuto Hoshi,[1] Tsuyoshi Takato,[1] Kozo Nakamura,[1] Sakae Tanaka,[1] Hiroto Okayama,[2] and Hiroshi Kawaguchi[1]

ABSTRACT: This study investigated the involvement of cell cycle factors in RANKL-induced osteoclast differentiation. Among the G1 cell cycle factors, Cdk6 was found to be a key molecule in determining the differentiation rate of osteoclasts as a downstream effector of the NF-κB signaling.

Introduction: A temporal arrest in the G1 phase of the cell cycle is a prerequisite for cell differentiation, making it possible that cell cycle factors regulate not only the proliferation but also the differentiation of cells. This study investigated cell cycle factors that critically influence differentiation of the murine monocytic RAW264.7 cells to osteoclasts induced by RANKL.

Materials and Methods: Growth-arrested RAW cells were stimulated with serum in the presence or absence of soluble RANKL (100 ng/ml). Expressions of the G1 cell cycle factors cyclin D1, D2, D3, E, cyclin-dependent kinase (Cdk) 2, 4, 6, and Cdk inhibitors (p18 and p27) were determined by Western blot analysis. Involvement of NF-κB and c-*jun* N-terminal kinase (JNK) pathways was examined by overexpressing dominant negative mutants of the *IκB kinase 2* (IKK^{DN}) gene and *mitogen-activated protein kinase kinase 7* ($MKK7^{DN}$) gene, respectively, using the adenovirus vectors. To determine the direct effect of Cdk6 on osteoclast differentiation, stable clones of RAW cells transfected with *Cdk6* cDNA were established. Osteoclast differentiation was determined by TRACP staining, and cell cycle regulation was determined by BrdU uptake and flow cytometric analysis.

Results and Conclusion: Among the cell cycle factors examined, the Cdk6 level was downregulated by RANKL synchronously with the appearance of multinucleated osteoclasts. Inhibition of the NF-κB pathway by IKK^{DN} overexpression, but not that of the JNK pathway by $MKK7^{DN}$ overexpression, caused the decreases in both Cdk6 downregulation and osteoclastogenesis by RANKL. RAW cells overexpressing Cdk6 resist RANKL-induced osteoclastogenesis; however, cell cycle regulation was not affected by the levels of Cdk6 overexpression, suggesting that the inhibitory effect of Cdk6 on osteoclast differentiation was not exerted through cell cycle regulation. These results indicate that Cdk6 is a critical regulator of RANKL-induced osteoclast differentiation and that its NF-κB–mediated downregulation is essential for efficient osteoclast differentiation.
J Bone Miner Res 2004;19:1128–1136. Published online on May 24, 2004; doi: 10.1359/JBMR.040513

Key words: osteoclast, cyclin, cell cycle, RANKL, bone

INTRODUCTION

OSTEOCLASTS ARE DERIVED from hematopoietic myeloid precursors of monocyte/macrophage lineage under the control of systemic and local factors produced by supporting cells such as osteoblasts and bone marrow stromal cells. Among these factors, RANKL is a TNF-related cytokine that stimulates osteoclast differentiation from hematopoietic precursor cells both in vitro and in vivo.[1–3] Mice lacking in either RANKL or its receptor RANK have defects in osteoclast differentiation that lead to severe osteopetrosis.[4–6] RANK is expressed on the surface of osteoclast progenitor cells and induces intracellular signals, leading to osteoclastogenesis on ligand binding or agonistic anti-RANK antibody stimulation.[6,7] Like other TNF receptor superfamily members, RANK stimulation can induce NF-κB, probably through association with several TNF receptor–associated factors (TRAFs): TRAF2, TRAF5, and TRAF6.[6,8–11] Mice deficient in both p50 and p52 subunits of NF-κB have been found to be osteopetrotic because of the failure in osteoclast differentiation, indicating a crucial role of NF-κB in osteoclastogenesis.[12,13] NF-κB activation requires sequential phosphorylation, ubiquitination, and degradation of the inhibitory subunit IκB as well as consequent exposure of a nuclear localization signal on NF-κB.[14–16] IκB kinase (IKK) signalsome is the protein complex that contains the inducible IκB kinase activity and consists of IKK1 (IKKα), IKK2 (IKKβ), and the NF-κB essential modulator (NEMO

The authors have no conflict of interest.

[1]Department of Sensory and Motor System Medicine, The University of Tokyo Graduate School of Medicine, Tokyo, Japan; [2]Department of Biochemistry and Molecular Biology, The University of Tokyo Graduate School of Medicine, Tokyo, Japan.

or IKK-γ). Among these three components of IKK signalsome, both IKK1 and IKK2 seem to play a critical role in IκB phosphorylation. However, the studies of IKK1 and IKK2 knockout mice indicate that IKK2 is more potent for NF-κB activation by proinflammatory stimuli than IKK1.[17–20] This evidence suggests that IKK2 may have a vital function in RANKL-induced NF-κB activation, and in fact, we previously reported that the dominant negative IKK2 ($IKK2^{DN}$) overexpression suppressed both NF-κB activity and osteoclast formation induced by RANKL using the murine monocytic RAW264.7 cell culture.[21]

Proliferation of eukaryotic cells depends on their progression through the cell cycle, and at least a temporal cell cycle arrest at the G1 phase is thought to be a prerequisite for cell differentiation.[22] Cell cycle control is achieved through the actions of a family of cyclins and cyclin-dependent protein kinases (Cdk's), which phosphorylate and thereby activate cell cycle factors essential for the onset of the next cell cycle phase. In mammalian cells, traverse through G1 and subsequent S phase entry require the activities of the cyclin D-dependent kinases Cdk4 and/or Cdk6 and the cyclin E-dependent kinase Cdk2. These Cdk's are negatively regulated by inhibitory proteins (CKIs) through direct binding to themselves.[23,24] CKIs have been classified into two families: INK4 and Cip/Kip. INK4 (p16, p15, p18, and p19) inhibits only Cdk4 and Cdk6, whereas Cip/Kip (p21, p27, and p57) inhibits all the Cdk's except for the Cdk6-cyclin D3 complex.[25] Because the control of cell cycle factors driving S phase onset greatly influences the commitment to cell differentiation in lower eukaryotes, this study investigated the possibility of crucial participation of some cell cycle start factors in RANKL-induced osteoclast differentiation and found that on RANKL treatment Cdk6 was downregulated primarily by RANKL/NF-κB signal-invoked transcriptional repression and that its downregulation was essential for efficient osteoclast differentiation.

MATERIALS AND METHODS

Reagents and antibodies

Human soluble recombinant RANKL was purchased from Wako Pure Chemicals (Osaka, Japan). Recombinant human macrophage-colony stimulating factor (M-CSF) was purchased from R&D Systems (Minneapolis, MN, USA). Antibodies against Cdk2 (H-298), Cdk4 (C-22), Cdk6 (C-21), cyclin D1 (C-20), cyclin D2 (M-20), cyclin D3 (C-16), cyclin E (M-20), p18 (M-20), p27 (F-8), mitogen-activated protein kinase kinase 7 (MKK7; MEK7), and IKK2 (H-470) were purchased from Santa Cruz Biotechnology (Santa Cruz, CA, USA). Antibodies against β-actin (AC-15) were purchased from Sigma Chemical (St Louis, MO, USA). DMEM and FBS were also purchased from Sigma Chemical. αMEM was purchased from Life Technologies (Rockville, MD, USA).

Cell culture and osteoclast differentiation assay

The RAW264.7 cell line was purchased from the Riken Cell Bank (Tsukuba, Japan). The cells were inoculated at 5×10^4 cells in a 6-well plate or 5×10^5 cells in a 10-cm plate and were cultured with DMEM containing 10% FBS at 37°C in 5% CO_2 in air. For osteoclast differentiation assay, RAW cells were grown in DMEM containing 10% FBS for 16–24 h. The culture medium was changed to DMEM containing 0.5% FBS, and the cells were cultured under serum starvation for 24–48 h. The growth-arrested RAW cells were stimulated with 10% FBS in the presence or absence of RANKL (100 ng/ml) for 1–7 days, fixed with 3.7% (vol/vol) formaldehyde in PBS), and stained at pH 5.0 in the presence of L(+)-tartaric acid using 3-hydroxy-2-naphthoic acid 2,4-dimethylanilide phosphate (Sigma) in *N,N*-dimethyl formamide (Sigma) as the substrate. $TRACP^+$ cells containing more than three nuclei were counted as osteoclasts.

For studies on primary osteoclast precursors, we used the M-CSF–dependent bone marrow macrophage (M-BMMϕ) culture system as described previously.[26] Briefly, bone marrow cells from 8-week-old male ddY mice (Sankyo Laboratories Animal Center, Tokyo, Japan) were seeded at 2×10^6 cells in a 6-multiwell plate and cultured in αMEM containing 10% FBS with M-CSF (10 ng/ml). After 2 days, adherent cells were used as M-BMMϕ after washing out the nonadherent cells including lymphocytes. The cells were then cultured in αMEM containing 0.5% FBS for 24 h and were further cultured in the presence of M-CSF (10 ng/ml) and RANKL (100 ng/ml) for 4 days. This experiment was performed according to the protocol approved by the Animal Care and Use Committee of the University of Tokyo.

Western blot analysis

Cells were rinsed with ice-cold PBS and lysed with RIPA buffer (100 μl for a well in 6-multiwell plate or 500 μl for a 10-cm plate) containing 10 mM Tris-HCl (pH 7.5), 150 mM NaCl, 1% Nonident-P40 (NP-40), 0.1% SDS, 10 μg/ml aprotinin, 0.1 M NaF, 2 mM Na_3VO_4, and 10 mM β-glycerophosphate. The cell lysates were sonicated briefly and clarified by centrifugation at 15,000*g* for 20 minutes at 4°C. The protein concentration in the cell lysate was measured using a Protein Assay Kit II (Bio-Rad). Equivalent amounts (10 μg) of cell lysate were electrophoresed by 7.5%, 10%, or 12.5% SDS-PAGE according to the molecular size of the proteins to be detected and were electrotransferred to polyvinylidene difluoride membranes (Immobilon-P; Millipore, Bedford, MA, USA). After blocking nonspecific binding with 5% skim milk, proteins were immunoblotted with respective antibodies and visualized using the ECL Plus Western Blotting Detection System (Amersham Pharmacia Biotech, Buckinghamshire, UK), following the manufacturer's instructions. Signals were quantified by densitometry (Bio-Rad). Experiments were performed at least three times, and a representative blotting was presented.

Transduction of $IKK2^{DN}$ and $MKK7^{DN}$ using adenovirus

The recombinant adenovirus vectors carrying the $IKK2^{DN}$ (Ser177 and Ser181 to Ala; $AxIKK2^{DN}$) and the β-*galactosidase* gene (AxLacZ) were kindly provided by Inder Verma (Salk Institute, La Jolla, CA, USA) and Izumu Saito (Tokyo University), respectively. The recombinant

adenovirus vector carrying kinase negative MKK7 (AxMKK7^{DN}, replaced ATP-binding lysine with glutamate residue) was constructed as described.[21] Preparation and infection of AxIKK2^{DN}, AxMKK7^{DN}, and AxLacZ were performed as previously reported.[21] Titers of the viral stock were determined by modified endpoint cytopathic effect assay with the following modifications. Fifty microliters of DMEM containing 10% FBS was dispensed into each well of a 96-well tissue culture plate, and eight rows of 3-fold serial dilutions of the virus starting from 10^{-4} dilutions were prepared. HEK293 cells (3×10^5) in 50 μl of DMEM containing 10% FBS were added to each well. The plate was incubated at 37°C in 5% CO_2 in air, and 50 μl of DMEM containing 10% FBS was added to each well every 3 days. Twelve days later, the endpoint of the cytopathic effect was determined by microscopy, and the 50% tissue culture infectious dose ($TCID_{50}$) was calculated. One $TCID_{50}$ per milliliter approximately corresponds to one plaque-forming unit (PFU) per milliliter. The multiplicity of infection (MOI) is expressed as a measure of titer of how many PFUs are added to every cell. Infection of adenovirus vectors to RAW cells was carried out as follows. The cells were inoculated at the density of 5×10^4 cells per 6-well plate and incubated for 20 h with DMEM containing 10% FBS at 37°C. After further incubation with a small amount of DMEM containing the recombinant adenovirus for 2 h at 37°C at 100 MOI, the cells were washed twice with PBS and again incubated in DMEM containing 10% FBS. Experiments were performed 2 days after the infection.

Establishment of RAW cells stably transfected with Cdk6

RAW cells were inoculated at the density of 5×10^5 cells per 6-cm plate, incubated for 24 h, and transfected with pEF/neoI that carries human *Cdk6* cDNA[25] using LipofectAMINE reagent (Life Technologies) following the manufacturer's instructions. Twenty-four hours after transfection, the cells were passaged 1:10–1:100 into DMEM containing 10% FBS and 400 μg/ml G418 (Geneticin; Life Technologies) for stable expression. After colony formation, each colony was isolated and passaged. We picked up more than 100 drug-resistant colonies, each of which was derived from a single clone. The expression levels of Cdk6 were quantified by Western blotting, and 12 high-expressing clones and 10 low-expressing clones were established.

RT-PCR

Total RNA (1 μg) was extracted from RAW cells using ISOGEN (Wako Pure Chemicals, Osaka, Japan) following the manufacturer's instructions, reverse transcribed using SUPERSCRIPT First-Strand Synthesis System for RT-PCR (Life Technologies), and amplified within an exponential phase of the amplification with a Perkin Elmer PCR Thermal Cycler (PE-2400). Gene-specific primer pairs were as follows: 5′-GCAACCTCCAGTCAGCA-3′ and 5′-GAAGTCACAGCCCTCAGAATC-3′ for RANK and 5′-CATGTAGGCCATGAGGTCCACCAC-3′ and 5′-TGAAGGTCGGTGTGAACGGATTTGGC-3′ for GAPDH. The cycling parameters were 30 s at 94°C, 30 s at 49°C, and 90 s at 72°C for RANK and 30 s at 94°C, 30s at 55°C, and 90 s at 72°C for GAPDH. Each band intensity was quantified by densitometry (Bio-Rad).

Flow cytometric analysis

About 1×10^5 cells were suspended in 0.02 ml citrate buffer, to which was added 0.18 ml Soln. A (0.03 mg/ml trypsin, 3.4 mM trisodium citrate, 0.1% NP40, 1.5 mM Spermine 4 HCl, and 0.5 mM Tris-HCl [pH 7.6]) and incubated for 10 minutes, and then added with 0.15 ml Soln. B (3.4 mM trisodium citrate, 0.1% NP40, 1,5 mM Spermine 4 HCl, 0.5 mM Tris-HCl [pH 7.6], 0.5 mg/ml trypsin inhibitor, 0.1 mg/ml Ribonuclease A) and incubated for 10 minutes; 0.15 ml Soln. C (4.16 mg/ml propidium iodite, 3.4 mM trisodium citrate, 0.1% NP40, 4.8 mM Spermine 4 HCl, 0.5 mM Tris-HCl [pH 7.6]) was finally added, and the mixture was again incubated for 10 minutes. All procedures were performed at room temperature. The DNA content was analyzed by EPICS XL (Beckman), and the data were analyzed by XL EXPO32 (Beckman).

BrdU incorporation assay

RAW cells were inoculated at a density of 1×10^3 cells per well in a 96-well plate and cultured in DMEM containing 10% FBS with or without hRANKL (100 ng/ml). At 3 days of culture, cells were labeled with BrdU for 2 h, and cell proliferation was determined by BrdU incorporation using a kit (Cell Proliferation ELISA; Roche Molecular Biochemical, Mannheim, Germany) following the manufacturer's instructions.

Statistical analysis

Means of groups were compared by ANOVA, and significance of differences was determined by posthoc testing using the Bonferroni method.

RESULTS

Cdk6 is downregulated by RANKL in RAW cells

We initially confirmed that RAW cells differentiated into TRACP$^+$ multinucleated osteoclasts after 5 days of treatment with soluble RANKL (100 ng/ml; Fig. 1A). We analyzed the regulation by RANKL of cell cycle factors that critically regulate the onset of S phase: Cdk2, Cdk4, Cdk6, cyclins (D1, D2, D3, and E), and CKIs (p18, p21, and p27) in RAW cells (Figs. 1B and 1C). Western blot analysis revealed that the Cdk6 protein level was decreased by RANKL after 5 days of culture and thereafter, whereas those of cyclins were hardly affected throughout the culture period up to 7 days. Although Cdk4 and Cdk6 have about 70% homology of amino acid sequence[27] and share D cyclins as their catalytic partners, only Cdk6 was regulated by RANKL. Levels of Cdk2, p18, and p27 were somewhat decreased by RANKL treatment, and neither p21 nor p57 was detected throughout the experiments in this cell line (data not shown).

To investigate whether the Cdk6 downregulation is specific to this cell line or a more general phenomenon, we performed the same Western blot analysis with a culture of

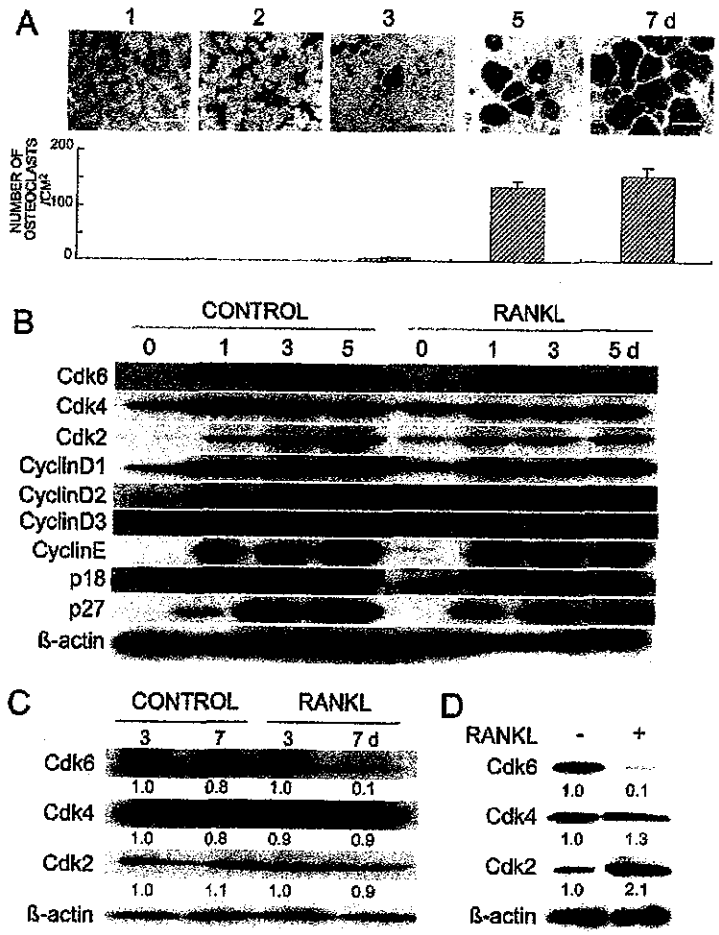

FIG. 1. (A) Time course of osteoclastogenesis from murine monocytic RAW264.7 cells, (B and C) expression of cell cycle factors by RANKL in the RAW264.7 cell culture, and (D) the murine primary osteoclast precursor M-BMMϕ culture. Cells were stimulated with serum in the presence or absence of RANKL (100 ng/ml) for the indicated days. (A) Osteoclastogenesis formed from cultured RAW cells was determined by TRACP staining, and the number of positively stained cells containing more than three nuclei was counted. Bar, 400 μm. The graph is expressed as means (bars) ± SE (error bars) for 8 wells/group. (B–D) The protein levels of cell cycle factors controlling the G1-S transition were determined at the indicated days of culture by Western blot analysis. β-actin was used as a loading control. B and C are from different cultures of RAW cells to confirm the regulation of Cdk's. D is from the M-BMMϕ culture for 4 days. The number under each band is the treated/control ratio of the intensity of each band normalized to that of β-actin measured by densitometry. In each figure a representative blotting was shown among at least three independent experiments that showed similar results.

primary osteoclast precursor M-BMMϕ. Treatment with RANKL inhibited induction of Cdk6 at 4 days, whereas Cdk4 was uninfluenced (Fig. 1D). Cdk2 was not decreased but was rather increased in this culture system. These results show that Cdk6 was specifically downregulated during the commitment to RANKL-induced osteoclast differentiation.

NF-κB mediates RANKL-induced downregulation of Cdk6

To examine the mediation of the NF-κB pathway, a major signaling pathway of RANKL, in the downregulation of Cdk6, we overexpressed $IKK2^{DN}$ in RAW cells using an adenovirus vector and examined its effect on RANKL-led Cdk6 downregulation. In our previous report, we confirmed that the adenovirus vector could efficiently transduce the $IKK2^{DN}$ gene into RAW cells and specifically suppressed the NF-κB activation in response to RANKL.[21] Both the inhibition of Cdk6 and the induction of osteoclastogenesis by RANKL were markedly reversed by the $IKK2^{DN}$ overexpression in RAW cells, whereas the control LacZ adenovirus infection did not affect the RANKL actions (Fig. 2A). These results indicate that the NF-κB signaling mediates not only osteoclast differentiation, but also the Cdk6 downregulation by RANKL.

We further investigated the possible involvement of the *c-jun* N-terminal kinase (JNK), another major signaling pathway of RANKL, in the downregulation of Cdk6 by RANKL. We previously reported that MKK7 is a vital function in JNK activation and osteoclast formation induced by RANKL, because $MKK7^{DN}$ overexpression using an adenovirus vector suppressed both of them.[21] Thus, we examined the effect of the adenovirus-mediated $MKK7^{DN}$ overexpression on RANKL-led Cdk6 downregulation in RAW cells. The $MKK7^{DN}$ overexpression suppressed the induction of osteoclastogenesis by RANKL as previously reported[21]; however, it did not restore the inhibition of Cdk6 in response to RANKL, unlike $IKK2^{DN}$ overexpression (Fig. 2B), indicating that the RANKL-led Cdk6 downregulation was not mediated by the JNK signaling.

RAW cells overexpressing Cdk6 resist RANKL-induced differentiation

As shown above, Cdk6 downregulation occurred during RANKL-induced osteoclast differentiation. Consequently, a critical question is whether or not this downregulation is essential for osteoclast differentiation. To address this, we generated RAW cell clones stably expressing various levels of Cdk6 by transfecting with an expressing vector harboring

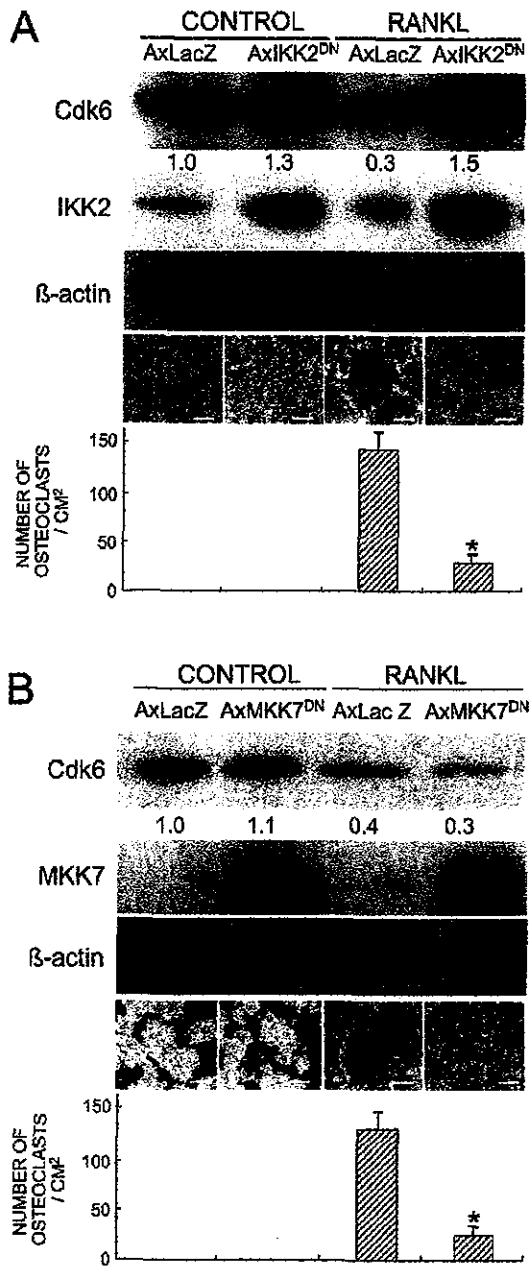

FIG. 2. Effects of overexpression of (A) IKK^{DN} and (B) $MKK7^{DN}$ *using adenovirus vectors* on the Cdk6 inhibition and osteoclastogenesis by RANKL in the RAW cell culture. RAW cells were infected with a recombinant adenovirus carrying the IKK^{DN}, $MKK7^{DN}$, or *LacZ* gene at 100 MOI, and subsequently, growth-arrested by incubation in a low serum medium for 2 days. The cells were stimulated with serum in the presence or absence of RANKL (100 ng/ml) for 5 days. Bar, 100 μm. Expressions of Cdk6, IKK2, and MKK7 were determined by Western blotting with β-actin as loading controls. The number under each band is the treated/control ratio of the intensity of the Cdk6 band normalized to that of β-actin measured by densitometry. Similar results were obtained in independent Western blottings of three separate experiments. The graph indicates means (bars) ± SE (error bars) for 8 wells/group. *Significant difference from the RANKL-treated and AxLacZ-infected culture; $p < 0.01$.

Cdk6 cDNA and tested their ability to respond to RANKL and differentiate to osteoclasts. The ability of RANKL to induce $TRACP^+$ multinucleated osteoclast formation was compared among the empty vector-transfected cells and low- (~1.5-fold) and high- (>5-fold) expressing cells. RANKL induced osteoclastogenesis in the empty vector-transfected cells and low-expressing clones; however, it was markedly decreased in high-expressing clones (Fig. 3A). Cdk6-led resistance to osteoclast differentiation is unlikely to be caused by an unexpected interference of the RANKL/NF-κB signaling by the overexpressed Cdk6, because RANK expression was not significantly affected by Cdk6 expression (Fig. 3B).

Overexpression of Cdk6 does not influence cell cycle regulation of osteoclasts

Because Cdk6 promotes the G1-S transition, suppression of osteoclast differentiation by overexpressed Cdk6 could be a mere consequence of its execution of this role. We therefore examined the effects of both RANKL and Cdk6 overexpression on G1-S transition and proliferation of RAW cells. The three kinds of transfected cells were similarly arrested in quiescence, stimulated with serum in the presence and absence of RANKL, and analyzed for cell proliferation and populations in G0/G1 and G2/M by BrdU incorporation and flow cytometric analysis (FACS; Table 1). At 3 days of culture, when osteoclastogenesis just started, RANKL slightly reduced cell proliferation and the G2/M population; however, Cdk6 overexpression caused no significant changes in either of them. These results indicate that the inhibitory effect of Cdk6 on osteoclast differentiation was not exerted through cell cycle regulation.

DISCUSSION

This study showed that Cdk6 is a key molecule in determining the differentiation rate of osteoclasts as a downstream effector of RANKL/NF-κB signaling. Figure 4 shows the mechanism of effect of RANKL on osteoclast differentiation based on present and previous studies. The RANK activation by binding of RANKL stimulates the NF-κB signaling, probably through association with TRAFs.[6,8–11] NF-κB moves from the cytoplasm into the nucleus, associates with various transcription factors in the nucleus, and downregulates Cdk6, which is a negative regulator of the transition from the G1 to the differentiation stage.

This study failed to show the contribution of JNK, another major pathway lying downstream of RANKL, to the RANKL-led Cdk6 downregulation. Our results, however, do not rule out the possibility that pathways other than NF-κB–mediated Cdk6 inhibition are required for osteoclast differentiation. JNK is known to activate activator protein 1 (AP-1), which is composed of various combinations of Fos and Jun family members. Mice deficient in c-*Fos* are reported to be osteopetrotic because of the failure in osteoclast differentiation, which can be rescued by Fra-1 as well as c-*Fos* overexpression,[28–31] indicating a crucial role of the JNK/AP-1 signaling in osteoclastogenesis.[12,13] JNK is activated by the phosphorylation of Thr and Tyr residues through MKK4 and/or MKK7. MKK7 seems to be

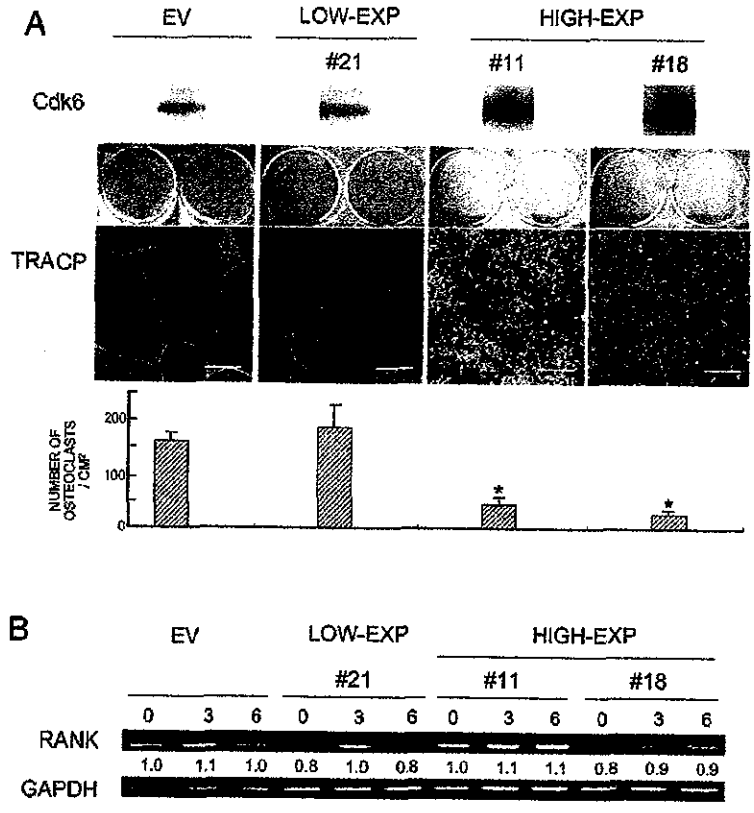

FIG. 3. (A) RANKL-induced osteoclastogenesis from RAW cells overexpressing Cdk6. Stable clones of RAW cells transfected with *Cdk6* cDNA were established as described in the Materials and Methods section, and clones with low expression (21) and high expression (11 and 18) were selected on Western blotting (top panel). These clones and empty vector-transfected RAW (EV) cells were induced for osteoclast differentiation by treating with RANKL (100 ng/ml) for 7 days, and osteoclast formation was determined by TRACP staining. The macroscopic images of culture wells and the microscopic images inside the wells are shown in the middle panels. Bar, 100 μm. The graph in the bottom panel is expressed as means (bars) ± SE (error bars) for 8 wells/group. *Significant difference from the EV cell culture; $p < 0.01$. (B) RANK mRNA levels by RT-PCR in each clone stimulated for 3 and 6 days with RANKL. The number under each band is the intensity of the RANK band normalized to that of GAPDH measured by densitometry. Other clones with low and high expressions showed similar results.

TABLE 1. CELL CYCLE REGULATION OF RAW CELLS OVEREXPRESSING Cdk6

	BrdU (OD)		*FACS*			
			G0/G1 (%)		*G2/M (%)*	
	RANKL⁻	*RANKL⁺*	*RANKL⁻*	*RANKL⁻*	*RANKL⁻*	*RANKL⁺*
EV	0.52 ± 0.03	0.39 ± 0.03*	75.2 ± 0.5	78.7 ± 0.7	15.9 ± 0.6	12.3 ± 0.6†
#21 (Low)	0.52 ± 0.05	0.34 ± 0.04*	75.5 ± 0.2	78.0 ± 0.4	16.1 ± 0.5	12.6 ± 0.5†
#11 (High)	0.56 ± 0.10	0.45 ± 0.03†	74.8 ± 0.9	78.9 ± 0.7	16.3 ± 0.9	12.2 ± 0.8†
#18 (High)	0.56 ± 0.08	0.39 ± 0.06†	75.7 ± 0.6	77.9 ± 0.9	16.7 ± 1.1	11.9 ± 0.6†

Cell proliferation was determined by BrdU incorporation into EV, low-expressing and high-expressing clones in the presence and absence of RANKL at 3 days of culture. Cell cycle distribution of mononuclear cells was determined by FACS, and percentages of cells in each cell cycle stage (G0/G1 and G2/M) are shown. Data are expressed as the mean ± SD for 6 wells/clone. Cdk6 overexpression did not significantly affect the cell proliferation and the cell cycle distribution. RANKL treatment reduced the cell proliferation and the cell population at G2/M.

*$p < 0.001$; †$p < 0.01$ significant inhibition by RANKL.

more specific in JNK activation than MKK4 because MKK4 is known to activate p38 MAPK as well. We previously reported that overexpression of $MKK7^{DN}$ in RAW cells by the adenovirus vector inhibited both RANKL-induced JNK activation and osteoclast formation.[21] JNK may possibly contribute to osteoclast differentiation through an independent pathway of Cdk6. Other possible pathways for osteoclast differentiation are the p38 MAPK and the Smad signaling. Recently, Matsumoto et al.[32] reported that RANKL activates p38 pathways in osteoclast precursors, which is essential for osteoclast differentiation, and Fuller et al.[33] and Kaneda et al.[34] showed the critical role of transforming growth factor (TGF)-β in osteoclast differentiation and survival. The involvement of cell cycle factors in osteoclast differentiation mediated by these pathways should be clarified in the future.

Cdk6 overexpression did not affect cell cycle regulation of RAW cells. D cyclins and partner kinases Cdk4 and Cdk6 are all known to be critical factors that control the cell growth potential,[35,36] but several specific roles have been reported for Cdk6. The Cdk6-cyclin D3 complex is unique among cyclin D and cognate kinase combinations and

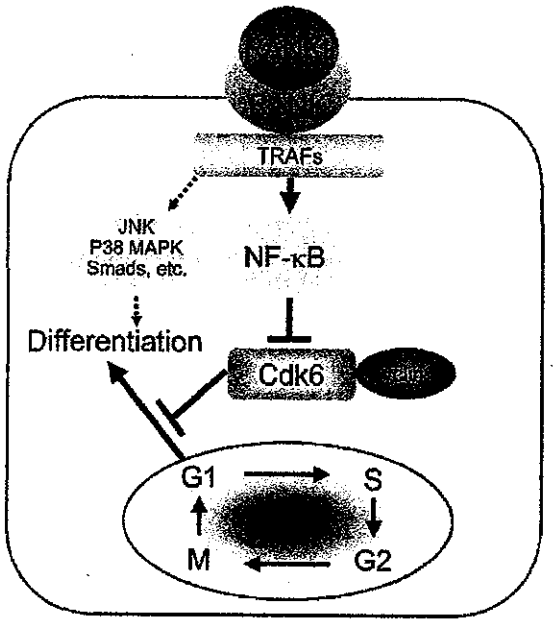

FIG. 4. Scheme of Cdk6-dependent RANKL effect on osteoclast differentiation obtained from this study. RANKL stimulates NF-κB signaling by binding to RANK through association with TRAFs. NF-κB downregulates Cdk6, which is a negative regulator of the transition from the G1 phase to the differentiation stage. Other signaling pathways such as JNK, p38 MAPK, and Smads might be involved in osteoclast differentiation through mechanisms independent of Cdk6.

evades inhibition by CKIs.[25] Therefore, it can greatly enhance the proliferative potential of fibroblasts under growth-suppressive conditions,[25] and consequently, sensitizes cells to physical and chemical transformation.[37] Cdk6 combined with cyclin K, encoded by human herpes virus 8, which is the causative agent of Kaposi sarcoma, is also reported to be immune to inhibition by CKIs.[38] These functions were not seen in Cdk4 complexes. This study discovered a novel function of Cdk6 as an inhibitor of the transition to the differentiation stage without affecting cell cycle regulation. Although Cdk4 has 70% homology of amino acid sequence with Cdk6,[27] the Cdk4 protein was not affected by RANKL in this study. We hereby propose that Cdk4 and Cdk6 play different roles and that Cdk4 cannot substitute for Cdk6 in osteoclastic cells.

How could Cdk6 control differentiation without influencing cell cycling? One possibility is that Cdk6 directly controls a factor critically involved in differentiation. This possibility may not be as remote as generally thought. In fission yeast, Pas1 cyclin and its partner kinase Pef1 activate a transcription factor complex functionally equivalent to E2F-DP of mammals, thereby promoting S phase entry, just like Cdk6, yet they independently inhibit the mating pheromone signaling whose activation is essential for differentiation of this yeast cell.[39] Thus, this might be a good model for the situation of Cdk6 in RANKL-induced osteoclast differentiation, highlighting a potential functional similarity between Cdk6 and Pef1.

Among cell cycle factors, Cdk's have vital roles in controlling cell cycle progression. Therefore, much attention has been devoted to the view that CKI-led inhibition of G1-specific Cdk's is critical for cell differentiation. Accordingly, potential roles for CKIs in differentiation have been studied extensively, but with mixed results.[40,41] Several studies revealed a certain correlation between induction of $p21^{CIP1}$ and differentiation in hematopoietic cells including monocytes/macrophages.[42–46] For osteoclast differentiation as well, upregulation of $p21^{CIP1}$ and $P27^{KIP1}$ is reported to be associated with osteoclast differentiation in the M-BMMϕ culture.[47] This was inconsistent with the present results in RAW cells that $P27^{KIP1}$ was not increased, but rather decreased, by RANKL and that $p21^{CIP1}$ could not be detected. Mice completely ablated for $p21^{CIP1}$ and/or $P27^{KIP1}$ or other major CKIs still develop and grow normally without significant bone abnormality such as osteopetrosis, strongly dismissing the current view.[41,48] Although there is evidence for $p57^{KIP2}$ being involved in differentiation of some cells,[49,50] no one has identified cell cycle factors that are controlled by differentiation signals and critically influence the differentiation commitment process. Because the Cdk6 downregulation was reproducible in RAW cell and M-BMMϕ cultures, we believe that Cdk6 generally plays a role in the RANKL-induced osteoclast differentiation. Although we tried to perform the signaling and overexpression experiments in M-BMMϕ, adenovirus infection and plasmid transfection were much less efficient in transducing these cells. Matsuo et al.[31] reported an efficient gene transfer into osteoclast precursors using a retrovirus vector system. However, the level of gene expression by retrovirus vectors is not enough for experiments using dominant negative molecules like this study. Developing more efficient gene transduction systems to primary osteoclast precursors will be helpful for further analysis of the signaling pathways of osteoclast differentiation.

This study for the first time showed that Cdk6, a G1 cell cycle factor, plays a critical role in controlling RANKL-induced osteoclast differentiation. Numerous signaling molecules, including transcription factors such as a nuclear factor of activated T-cells (NFATs),[51,52] have recently been reported to be involved in osteoclast differentiation. Consequently, one of these factors may be responsible for the RANKL-triggered repression of Cdk6 transcription. Identification of the transcriptional repressor as well as key targets for Cdk6 will definitely be required for deeper understanding of the molecular basis of bone resorption.

ACKNOWLEDGMENTS

We thank Reiko Yamaguchi for providing expert technical assistance and Drs Inder Verma and Izumu Saito for kindly providing adenovirus vectors carrying $IKK2^{DN}$ and LacZ, respectively. This study was funded by a Grant-in-Aid for Scientific Research from the Japanese Ministry of Education, Science, Sports, Culture and Technology (14657358).

REFERENCES

1. Suda T, Takahashi N, Udagawa N, Jimi E, Gillespie MT, Martin TJ 1999 Modulation of osteoclast differentiation and function by the new members of the tumor necrosis factor receptor and ligand families. Endocr Rev **20**:345–357.
2. Lacey DL, Timms E, Tan HL, Kelley MJ, Dunstan CR, Burgess T, Elliott R, Colombero A, Elliott G, Scully S, Hsu H, Sullivan J, Hawkins N, Davy E, Capparelli C, Eli A, Qian YX, Kaufman S, Sarosi I, Shalhoub V, Senaldi G, Guo J, Delaney J, Boyle WJ 1998 Osteoprotegerin ligand is a cytokine that regulates osteoclast differentiation and activation. Cell **93**:165–176.
3. Yasuda H, Shima N, Nakagawa N, Yamaguchi K, Kinosaki M, Mochizuki S, Tomoyasu A, Yano K, Goto M, Murakami A, Tsuda E, Morinaga T, Higashio K, Udagawa N, Takahashi N, Suda T 1998 Osteoclast differentiation factor is a ligand for osteoprotegerin/osteoclastogenesis-inhibitory factor and is identical to TRANCE/RANKL. Proc Natl Acad Sci USA **95**:3597–3602.
4. Kong YY, Boyle WJ, Penninger JM 1999 Osteoprotegerin ligand: A common link between osteoclastogenesis, lymph node formation and lymphocyte development. Immunol Cell Biol **77**:188–193.
5. Kong YY, Yoshida H, Sarosi I, Tan HL, Timms E, Capparelli C, Morony S, Oliveira-dos-Santos AJ, Van G, Itie A, Khoo W, Wakeham A, Dunstan CR, Lacey DL, Mak TW, Boyle WJ, Penninger JM 1999 OPGL is a key regulator of osteoclastogenesis, lymphocyte development and lymph-node organogenesis. Nature **397**:315–323.
6. Li J, Sarosi I, Yan XQ, Morony S, Capparelli C, Tan HL, McCabe S, Elliott R, Scully S, Van G, Kaufman S, Juan SC, Sun Y, Tarpley J, Martin L, Christensen K, McCabe J, Kostenuik P, Hsu H, Fletcher F, Dunstan CR, Lacey DL, Boyle WJ 2000 RANK is the intrinsic hematopoietic cell surface receptor that controls osteoclastogenesis and regulation of bone mass and calcium metabolism. Proc Natl Acad Sci USA **97**:1566–1571.
7. Nakagawa N, Kinosaki M, Yamaguchi K, Shima N, Yasuda H, Yano K, Morinaga T, Higashio K 1998 RANK is the essential signaling receptor for osteoclast differentiation factor in osteoclastogenesis. Biochem Biophys Res Commun **253**:395–400.
8. Darnay BG, Haridas V, Ni J, Moore PA, Aggarwal BB 1998 Characterization of the intracellular domain of receptor activator of NF-κB (RANK). Interaction with tumor necrosis factor receptor-associated factors and activation of NF-κB and c-Jun N-terminal kinase. J Biol Chem **273**:20551–20555.
9. Darnay BG, Ni J, Moore PA, Aggarwal BB 1999 Activation of NF-κB by RANK requires tumor necrosis factor receptor-associated factor (TRAF) 6 and NF-kappaB-inducing kinase. Identification of a novel TRAF6 interaction motif. J Biol Chem **274**: 7724–7731.
10. Galibert L, Tometsko ME, Anderson DM, Cosman D, Dougall WC 1998 The involvement of multiple tumor necrosis factor receptor (TNFR)-associated factors in the signaling mechanisms of receptor activator of NF-kappaB, a member of the TNFR superfamily. J Biol Chem **273**:34120–34127.
11. Lomaga MA, Yeh WC, Sarosi I, Duncan GS, Furlonger C, Ho A, Morony S, Capparelli C, Van G, Kaufman S, van der Heiden A, Itie A, Wakeham A, Khoo W, Sasaki T, Cao Z, Penninger JM, Paige CJ, Lacey DL, Dunstan CR, Boyle WJ, Goeddel DV, Mak TW 1999 TRAF6 deficiency results in osteopetrosis and defective interleukin-1, CD40, and LPS signaling. Genes Dev **13**:1015–1024.
12. Iotsova V, Caamano J, Loy J, Yang Y, Lewin A, Bravo R 1997 Osteopetrosis in mice lacking NF-kappaB1 and NF-kappaB2. Nat Med **3**:1285–1289.
13. Franzoso G, Carlson L, Xing L, Poljak L, Shores EW, Brown KD, Leonardi A, Tran T, Boyce BF, Siebenlist U 1997 Requirement for NF-kappaB in osteoclast and B-cell development. Genes Dev **11**:3482–3496.
14. Verma IM, Stevenson J 1997 IkappaB kinase: Beginning, not the end. Proc Natl Acad Sci USA **94**:11758–11760.
15. Karin M 1999 The beginning of the end: IkappaB kinase (IKK) and NF-kappaB activation. J Biol Chem **274**:27339–27342.
16. Ghosh S 1999 Regulation of inducible gene expression by the transcription factor NF-kappaB. Immunol Res **19**:183–189.
17. Li Q, Van Antwerp D, Mercurio F, Lee KF, Verma IM 1999 Severe liver degeneration in mice lacking the IkappaB kinase 2 gene. Science **284**:321–325.
18. Li Q, Lu Q, Hwang JY, Buscher D, Lee KF, Izpisua-Belmonte JC, Verma IM 1999 IKK1-deficient mice exhibit abnormal development of skin and skeleton. Genes Dev **13**:1322–1328.
19. Li ZW, Chu W, Hu Y, Delhase M, Deerinck T, Ellisman M, Johnson R, Karin M 1999 The IKKbeta subunit of IkappaB kinase (IKK) is essential for nuclear factor kappaB activation and prevention of apoptosis. J Exp Med **189**:1839–1845.
20. Rudolph D, Yeh WC, Wakeham A, Rudolph B, Nallainathan D, Potter J, Elia AJ, Mak TW 2000 Severe liver degeneration and lack of NF-kappaB activation in NEMO/IKKgamma-deficient mice. Genes Dev **14**:854–862.
21. Yamamoto A, Miyazaki T, Kadono Y, Takayanagi H, Miura T, Nishina H, Katada T, Wakabayashi K, Oda H, Nakamura K, Tanaka S 2002 Possible involvement of IkappaB kinase 2 and MKK7 in osteoclastogenesis induced by receptor activator of nuclear factor kappaB ligand. J Bone Miner Res **17**:612–621.
22. Sherr CJ 1994 G1 phase progression: Cycling on cue. Cell **79**: 551–555.
23. Sherr CJ, Roberts JM 1999 CDK inhibitors: Positive and negative regulators of G1-phase progression. Genes Dev **13**:1501–1512.
24. Vidal A, Koff A 2000 Cell-cycle inhibitors: Three families united by a common cause. Gene **247**:1–15.
25. Kobayashi K, Takahashi N, Jimi E, Udagawa N, Takami M, Kotake S, Nakagawa N, Kinosaki M, Yamaguchi K, Shima N, Yasuda H, Morinaga T, Higashio K, Martin TJ, Suda T 2000 Tumor necrosis factor alpha stimulates osteoclast differentiation by a mechanism independent of the ODF/RANKL-RANK interaction. J Exp Med **191**:275–286.
26. Lin J, Jinno S, Okayama H 2001 Cdk6-cyclin D3 complex evades inhibition by inhibitor proteins and uniquely controls cell's proliferation competence. Oncogene **20**:2000–2009.
27. Meyerson M, Enders GH, Wu CL, Su LK, Gorka C, Nelson C, Harlow E, Tsai LH 1992 A family of human cdc2-related protein kinases. EMBO J **11**:2909–2917.
28. Wang ZQ, Ovitt C, Grigoriadis AE, Mohle-Steinlein U, Ruther U, Wagner EF 1992 Bone and haematopoietic defects in mice lacking c-*fos*. Nature **360**:741–745.
29. Johnson RS, Spiegelman BM, Papaioannou V 1992 Pleiotropic effects of a null mutation in the c-fos proto-oncogene. Cell **71**: 577–586.
30. Grigoriadis AE, Wang ZQ, Cecchini MG, Hofstetter W, Felix R, Fleisch HA, Wagner EF 1994 c-Fos: A key regulator of osteoclast-macrophage lineage determination and bone remodeling. Science **266**:443–448.
31. Matsuo K, Owens JM, Tonko M, Elliott C, Chambers TJ, Wagner EF 2000 Fosl1 is a transcriptional target of c-Fos during osteoclast differentiation. Nat Genet **24**:184–187.
32. Matsumoto M, Sudo T, Saito T, Osada H, Tsujimoto M 2000 Involvement of p38 mitogen-activated protein kinase signaling pathway in osteoclastogenesis mediated by receptor activator of NF-kappa B ligand (RANKL). J Biol Chem **275**:31155–31161.
33. Fuller K, Lean JM, Bayley KE, Wani MR, Chambers TJ 2000 A role for TGFbeta(1) in osteoclast differentiation and survival. J Cell Sci **113**:2445–2453.
34. Kaneda T, Nojima T, Nakagawa M, Ogasawara A, Kaneko H, Sato T, Mano H, Kumegawa M, Hakeda Y 2000 Endogenous production of TGF-beta is essential for osteoclastogenesis induced by a combination of receptor activator of NF-kappaB ligand and macrophage-colony-stimulating factor. J Immunol **165**:4254–4263.
35. Baldin V, Lucas J, Marcote MJ, Pagano M, Draetta G 1993 Cyclin D1 is a nuclear protein required for cell cycle progression in G_1. Genes Dev **7**:812–821.
36. Hengstschlager M, Braun K, Soucek A, Miloloza E, Hengstschlager O 1999 Cyclin-dependent kinases at the G_1-S transition of the mammalian cell cycle. Mutat Res **436**:1–9.
37. Chen Q, Lin J, Jinno S, Okayama H 2003 Overexpression of Cdk6-cyclin D3 highly sensitizes cells to physical and chemical transformation. Oncogene **22**:992–1001.
38. Swanton C, Mann DJ, Fleckenstein B, Neipel F, Peters G, Jones N 1997 Herpes viral cyclin/Cdk6 complexes evade inhibition by CDK inhibitor proteins. Nature **390**:184–187.
39. Tanaka K, Okayama H 2000 A pcl-like cyclin activates the Res2p-Cdc10p cell cycle "start" transcriptional factor complex in fission yeast. Mol Biol Cell **11**:2845–2862.
40. Missero C, Di Cunto F, Kiyokawa H, Koff A, Dotto GP 1996 The absence of p21Cip1/WAF1 alters keratinocyte growth and differ-

entiation and promotes ras-tumor progression. Genes Dev **10:** 3065–3075.
41. Deng C, Zhang P, Harper JW, Elledge SJ, Leder P 1995 Mice lacking p21CIP1/WAF1 undergo normal development, but are defective in G1 checkpoint control. Cell **82:**675–684.
42. Steinman RA, Hoffman B, Iro A, Guillouf C, Liebermann DA, el-Houseini ME 1994 Induction of p21 (WAF-1/CIP1) during differentiation. Oncogene **9:**3389–3396.
43. Schwaller J, Koeffler HP, Niklaus G, Loetscher P, Nagel S, Fey MF, Tobler A 1995 Posttranscriptional stabilization underlies p53-independent induction of p21WAF1/CIP1/SDI1 in differentiating human leukemic cells. J Clin Invest **95:**973–979.
44. Freemerman AJ, Vrana JA, Tombes RM, Jiang H, Chellappan SP, Fisher PB, Grant S 1997 Effects of antisense p21 (WAF1/CIP1/MDA6) expression on the induction of differentiation and drug-mediated apoptosis in human myeloid leukemia cells (HL-60). Leukemia **11:**504–513.
45. Liu M, Lee MH, Cohen M, Bommakanti M, Freedman LP 1996 Transcriptional activation of the Cdk inhibitor p21 by vitamin D3 leads to the induced differentiation of the myelomonocytic cell line U937. Genes Dev **10:**142–153.
46. Muto A, Kizaki M, Yamato K, Kawai Y, Kamata-Matsushita M, Ueno H, Ohguchi M, Nishihara T, Koeffler HP, Ikeda Y 1999 1,25-dihydroxyvitamin D3 induces differentiation of a retinoic acid-resistant acute promyelocytic leukemia cell line (UF-1) associated with expression of p21(WAF1/CIP1) and p27(KIP1). Blood **93:**2225–2233.
47. Okahashi N, Murase Y, Koseki T, Sato T, Yamato K, Nishihara T 2001 Osteoclast differentiation is associated with transient upregulation of cyclin-dependent kinase inhibitors p21(WAF1/CIP1) and p27(KIP1). J Cell Biochem **80:**339–345.
48. Nakayama K, Ishida N, Shirane M, Inomata A, Inoue T, Shishido N, Horii I, Loh DY 1996 Mice lacking p27(Kip1) display increased body size, multiple organ hyperplasia, retinal dysplasia, and pituitary tumors. Cell **85:**707–720.
49. Yan Y, Frisen J, Lee MH, Massague J, Barbacid M 1997 Ablation of the CDK inhibitor p57Kip2 results in increased apoptosis and delayed differentiation during mouse development. Genes Dev **11:**973–983.
50. Zhang P, Liegeois NJ, Wong C, Finegold M, Hou H, Thompson JC, Silverman A, Harper JW, DePinho RA, Elledge SJ 1997 Altered cell differentiation and proliferation in mice lacking p57KIP2 indicates a role in Beckwith-Wiedemann syndrome. Nature **387:**151–158.
51. Takayanagi H, Kim S, Koga T, Nishina H, Isshiki M, Yoshida H, Saiura A, Isobe M, Yokochi T, Inoue J, Wagner EF, Mak TW, Kodama T, Taniguchi T 2002 Induction and activation of the transcription factor NFATc1 (NFAT2) integrate RANKL signaling in terminal differentiation of osteoclasts. Dev Cell **3:**889–901.
52. Ishida N, Hayashi K, Hoshijima M, Ogawa T, Koga S, Miyatake Y, Kumegawa M, Kimura T, Takeya T 2002 Large scale gene expression analysis of osteoclastogenesis in vitro and elucidation of NFAT2 as a key regulator. J Biol Chem **277:**41147–41156.

Address reprint requests to:
Hiroshi Kawaguchi, MD, PhD
Department of Orthopaedic Surgery
Faculty of Medicine
University of Tokyo
Hongo 7-3-1, Bunkyo
Tokyo 113-8655, Japan
E-mail: kawaguchi-ort@h.u-tokyo.ac.jp

Received in original form August 10, 2003; in revised form February 5, 2004; accepted March 11, 2004.

Conjugation of Enzymes on Polymer Nanoparticles Covered with Phosphorylcholine Groups

T. Konno, J. Watanabe, and K. Ishihara*

Department of Materials Engineering, School of Engineering, The University of Tokyo, 7-3-1, Hongo, Bunkyo-ku, Tokyo 113-8656, Japan

Received September 16, 2003; Revised Manuscript Received November 27, 2003

We investigated the bioconjugation of enzymes on polymer nanoparticles covered with bioinert phosphorylcholine groups. A water-soluble amphiphilic phospholipid polymer (PMBN) was specially designed for preparation of nanoparticles and conjugation with enzymes on them. The PMBN was prepared by random copolymerization of 2-methacryloyloxyethyl phosphorylcholine (MPC), *n*-butyl methacrylate, and *p*-nitrophenylester bearing methacrylate. The PMBN was used as an emulsifier and a surface modifier to prepare the poly(L-lactic acid) nanoparticles by a solvent evaporation technique in aqueous medium. The nanoparticles covered with phosphorylcholine groups were stably dispersed in an aqueous solution and a phosphate buffered saline. The diameter and surface ζ-potential of the nanoparticles were ca. 200 nm and −6 mV, respectively. The *p*-nitrophenyl ester groups, which are active ester units for the amino groups of the protein, were located at the surface of the nanoparticles. Both acetylcholine esterase and choline oxidase were co-immobilized (dual-mode conjugation) by the reaction between the *p*-nitrophenyl ester group and the amino group of these enzymes. The enzymatic reactions on the nanoparticles were followed using a microdialysis biosensor system with a microtype hydrogen peroxide electrode in the probe. The nanoparticles conjugated with these enzymes could detect the acetylcholine chloride as hydrogen peroxide, which is a product of the enzymatic reactions on the surface of the nanoparticles in the probe. Namely, continuous enzyme reactions could be occurring on the surface of the nanoparticles. It is concluded that the nanoparticles are a promising tool for a highly sensitive and microdiagnostic system.

Introduction

The purpose of this study is the preparation of polymer nanoparticles covered with a phosphorylcholine group and active ester groups (*p*-nitrophenyl ester groups) on the surface to conjugate specific biomolecules including proteins. We have already reported that the polymer nanoparticles covered with phosphorylcholine groups are inert biologically; that is, when they contact blood, they do not adsorb plasma proteins.[1] Also the polymer surface covered with phosphorylcholine groups inhibited the adhesion and activation of blood cells.[2−6]

Recently, polymer nanoparticles having directional antenna molecules such as enzymes and antibodies are expected to be novel diagnostic agents and targeting drug carriers to target specific cells and organs.[7,8] However, attention has not been paid to conventional polymer nanoparticles for the preparation of a suitable interface, which is the most important factor for antenna molecules to show their performance such as selectivity and reactivity. We hypothesized that the polymer nanoparticles covered with phosphorylcholine groups will provide a suitable platform to conjugate with specific biomolecules. Thus, if these biomolecules are located at an inert surface, they have good bioselectivity, specific reactivity, and so on.

In this study, a novel phospholipid polymer, poly[2-methacryloyloxyethyl phosphorylcholine (MPC)-*co*-*n*-butyl methacrylate (BMA)-*co*-*p*-nitrophenyloxycarbonyl poly(ethylene glycol) methacrylate (MEONP)] (PMBN) was synthesized. One of the monomer units, the MEONP unit, has an active ester group in the side chain, which can react with a specific biomolecule via condensation with an amino group of the biomolecule.[8,9] The polymer nanoparticles were prepared using the PMBN as an emulsifier and a surface modifier. The poly(L-lactic acid) (PLA) was used as a core substance where the surface was covered with PMBN chains (PMBN/PLA nanoparticles). Two kinds of enzymes, acetylcholine esterase (AChE) and choline oxidase (ChO), were co-immobilized (dual-mode conjugation) on the surface of the PMBN/PLA nanoparticles to achieve enzymatic reactions continuously. The enzymatic reactions on the nanoparticles were followed using a microdialysis biosensor system with a hydrogen peroxide electrode. The PMBN/PLA nanoparticles conjugated with enzymes were filled into the dialysis probe. We will discuss the detection of acetylcholine by the hydrogen peroxide electrode after the continuous enzymatic reactions on the polymer nanoparticles

Experimental Section

Materials. MPC was synthesized by the method reported previously.[10] Chloroform, acetonitrile, and triethylamine (TEA) were purchased from Kanto Chemical Co. Ltd.,

* To whom correspondence should be addressed. Phone: +81-3-5841-7124. Fax: +81-3-5841-8647. E-mail: ishihara@bmw.t.u-tokyo.ac.jp.

10.1021/bm034356p CCC: $27.50
Published on Web 01/09/2004

Tokyo, Japan, and purified by distillation under reduced pressure. Poly(ethylene glycol) monomethacrylate (MEOnOH) was obtained from NOF Co., Ltd., Tokyo, Japan, (as Blenmer PE−200) and used without further purification. The average number of oxyethylene repeating units in MEOnOH was 4.5, which was determined by ^{1}H NMR (JEOL JNM-GX 270, Tokyo, Japan) spectroscopy. *p*-Nitrophenylchloroformate was purchased from Sigma-Aldrich, Corp., St. Louis, MO. PLA (Average molecular weight: 2.0×10^4), AChE (from Bovine erythrocytes, EC 3.1.1.7), ChO (from Alcaligenes sp. EC 1.1.3.17), acetylcholine chloride, and choline chloride were purchased from Wako Pure Chemical Industries Co. Ltd., Osaka, Japan, and used without further purification. The other reagents and solvents were commercially available reagents of extra-pure grade and were used without further purification.

Methods

Monomer Synthesis (MEONP). Into a 300-mL four-necked round-bottomed flask equipped with a dropping funnel, a thermometer, and a magnetic stirrer were placed Blenmer PE−200 (22.2 g) and TEA (7.9 g), and then 50 mL of chloroform was added to the mixture. After the solution was cooled at −30 °C, *p*-nitrophenylchloroformate (15.7 g) dissolved in 40 mL of chloroform was added drop by drop to the stirred solution over a period of 1 h. The temperature of the reaction mixture was maintained at −30 °C for 2 h. The precipitate formed in the reaction mixture was triethylamine hydrochloride (TEAC), which was then filtered off. The solvent in the filtrate was evaporated under reduced pressure. To the residue was added a small amount of dry diethyl ether to remove the dissolved TEAC, followed by filtration. By evaporation of the filtrate under reduced pressure, MEONP was obtained as a yellow oily liquid. The structure of MEONP was confirmed by Fourier transform-infrared measurement (FT-IR, FT-IR-500, Jasco Co., Ltd., Tokyo, Japan). IR(cm-1): 3081(p-Ar), 2870 (CH3-,-CH2-), 1770 (Ar−CO−O−R), 1720 (C=O), 1637 (C=C), 1348 (Ar−NO2), 860 (Ar−NO2).

Preparation of Water-Soluble Amphiphilic Phospholipid Polymer. Water-soluble amphiphilic phospholipid polymer (PMBN) with an MPC unit, a BMA unit, and an MEONP unit was prepared by conventional radical polymerization of the corresponding monomers using α,α′-azobisisobutyronitrile (AIBN) as an initiator. The MPC unit mole fraction in the PMBN was determined by ^{1}H NMR measurement (JEOL α-500 high-resonance spectrometer, Tokyo, Japan). The MEONP unit in the PMBN was determined from the concentration of *p*-nitrophenol (absorbance at 400 nm) released by hydrolysis of the polymer in 0.01 M NaOH aqueous solution with a UV spectrophotometer (V-550, Jasco Co., Ltd., Tokyo, Japan).

Preparation of Polymer Nanoparticles. The polymer nanoparticles having both phosphorylcholine groups and *p*-nitrophenyl ester groups on the surface were prepared by the solvent evaporation technique in aqueous medium, the same method as reported previously.[1] A brief explanation is as follows. The PMBN aqueous solution (40 mL) with a given concentration was placed in a glass bottle and stirred at 400 rpm. PLA (20 mg) was dissolved in methylene dichloride (2 mL). The PLA solution was dropped into the PMBN aqueous solution. The mixed solution was sonicated with a probe-type generator at 4 °C for 30 min. The formed suspension was kept under reduced pressure for 2 h to evaporate the methylene dichloride. The formed polymer nanoparticles were fractionated by centrifugation (Allegra 21R, Beckman-Coulter, Inc. U.S.A.) at 10 300 g and 4 °C for 30 min. The nanoparticles as the precipitate were collected and resuspended with distilled water to eliminate the excess PMBN. This procedure was repeated three times. The obtained polymer nanoparticles were called as PMBN/PLA nanoparticles.

Characterization of Polymer Nanoparticles. The PMBN/PLA nanoparticle suspension (100 μL, 10 mg/mL) was added in the 0.01 M NaOH aqueous solution (1 mL). The mixed solution was kept under room temperature for 3 h to completely hydrolyze the *p*-nitrophenyl ester groups. The PMBN/PLA nanoparticles were precipitated by centrifugation (10 300 g, 30 min, 4 °C). The UV adsorption of the supernatant was measured by a UV spectrophotometer. The spectrum of released *p*-nitrophenol (400 nm) was measured in the range of 300−600 nm, and the amount of *p*-nitrophenol released from the PMBN/PLA nanoparticles was determined by the UV absorbance at 400 nm. The surface analysis of the PMBN/PLA nanoparticles was carried out by X-ray photoelectron spectroscopy (XPS, AXIS−Hsi, Shimadzu/Kratos, Kyoto, Japan). The PMBN/PLA nanoparticle suspension was spread on a poly(ethylene terephthalate) (PET) plate and dried in vacuo. The PET plate covered with the PMBN/PLA nanoparticles was stored in the reference room. The takeoff angle of the photoelectrons was 90°.

One drop of suspension containing PMBN/PLA nanoparticles prepared in the 1.0 mg/mL PMBN solution was spread on a mica sheet. The mica sheet was dried in air at room temperature. The morphology of the PMBN/PLA nanoparticles was observed using an atomic force microscope (AFM, SPI-3800, Seiko Instrument Co., Ltd., Chiba, Japan). The tapping mode was applied for the AFM. The Laser-Doppler electrophoresis measurements were carried out using an ELS-8000 (Otsuka Electronics, Osaka, Japan) at 25 °C with an electrical field strength of 30−35 V/cm. This experiment was carried out in phosphate-buffered saline (PBS, pH 7.4, ionic strength 10 mM). The particle size and size distribution of the PMBN/PLA nanoparticles were determined by a dynamic light scattering measurement (DLS-7000, Ostuka Electronics).

Conjugation of Enzymes on the Polymer Nanoparticles. ChO (2 mg) was dissolved in 1 mL of the PMBN/PLA nanoparticle suspension (10 mg/mL) in PBS (pH 7.4). The mixed suspension was kept at 4 °C and stirred with a magnetic stirrer for 24 h. According to this procedure, the ChO was conjugated with the active ester unit on the surface of the polymer nanoparticles. After conjugation with ChO, the mixed suspension was centrifuged at 10 300 g, 30 min and 4 °C to eliminate the unbound ChO.

In the case of the dual-mode conjugation of enzymes on the PMBN/PLA nanoparticles, both CHO and AChE were

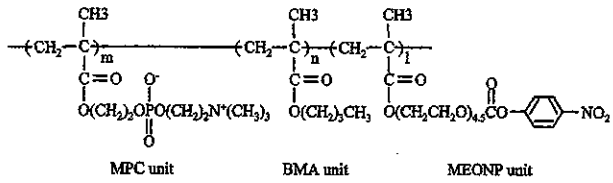

Figure 1. Chemical structure of PMBN.

dissolved in a 1 mg suspension of the polymer nanoparticles in PBS. The reaction conditions were the same as those for a single enzyme immobilization. The obtained polymer nanoparticles conjugated enzymes were immediately used for the following experiments.

Following the Enzymatic Reactions Using the Microdialysis Biosensor System. To follow the enzymatic reactions on the surface of the polymer nanoparticles, an amperometric microdialysis sensor system with a hydrogen peroxide electrode (EICOM Co., Ltd., Kyoto, Japan) was used. The degassed PBS as a perfusion solution was run into the dialysis hollow fiber probe using a syringe pump (rate: 0.2 μL/min). After filling the perfusion solution into the hollow fiber, the dialysis probe was cleaned by charging at −400 mV. After the current value was 0 mA, the PMBN/PLA nanoparticles conjugated with enzymes (10 mg/mL) were filled into the dialysis probe. Immediately, the dialysis probe was charged at +550 mV. After the current value reached 0 mA, choline chloride solution (1.5 mg/mL) or acetylcholine chloride solution (1.5 mg/mL) was added to 50 mL of the outer solution. The current value induced by the enzymatic reactions on the polymer nanoparticles was continuously recorded using a current detector.

Results and Discussion

The water-soluble amphiphilic phospholipid polymer (PMBN) for preparation of the polymer nanoparticles and bioconjugation of the enzyme on the surface was synthesized using MPC, BMA, and MEONP by a conventional radical polymerization. The chemical structure of PMBNs is shown in Figure 1.

The MPC unit is a hydrophilic and biocompatible moiety, the BMA unit was selected as a hydrophobic moiety to form stable polymer aggregates in water, and the MEONP unit has an active ester unit to bioconjugate with the enzymes. The synthetic results of various PMBNs are shown in Table 1.

The PMBN40 that has a 0.66 mol fraction of the MPC unit could be dissolved in water even where there is a 0.28 mol fraction of the hydrophobic BMA unit. In our previous article, an amphiphilic MPC polymer, poly(MPC-*co*-BMA),

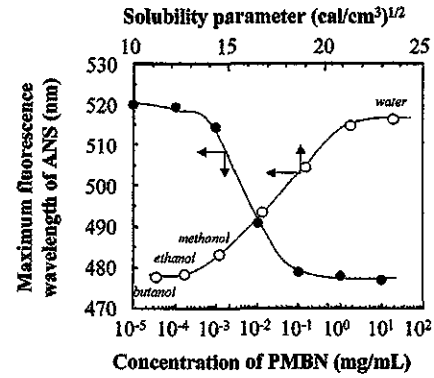

Figure 2. Concentration dependence of the maximum fluorescence wavelength of ANS in PMBN aqueous solution (closed circle), and the relationship between the solubility parameter of various solvents and the fluorescence wavelength of ANS (open circle).

could form an aggregate when it was dissolved in water.[11] That is, stable hydrophobic domains were formed in the aqueous medium. We considered that this phenomenon could be used for emulsionization of organic compounds to stabilize organic droplets in an aqueous medium. In this study, the water-soluble PMBN40 was used as an emulsifier and a surface modifier. The basic characterization of PMBN40 was evaluated using the fluorescence probe 1-anilino-8-naphthalene sulfonate (ANS). The fluorescence probe ANS was sensitive to the polarity of the solvent. When the ANS molecules were dissolved in a polar solvent like water, the maximum fluorescence wavelength was 510 nm. On the other hand, when the ANS molecules were dissolved in an apolar solvent, the maximum fluorescence wavelength was shifted toward a blue wavelength. For example, when the ANS molecules were dissolved in butanol, the maximum fluorescence wavelength was 475 nm. Figure 2 shows the maximum fluorescence wavelength of ANS in various concentrations of PMBN aqueous solution and the fluorescence wavelength of ANS in various solvents.

Because water-soluble PMBN has an amphiphilic character, it can form stable polymer aggregates in water. The ANS molecules were located in the hydrophobic domain of the polymer aggregates. It was indicated that the polarity (solubility parameter) of polymer aggregates almost corresponded to ethanol and butanol, and this result showed that the PMBN could be used as an emulsifier and surface modifier during preparation of the polymer nanoparticles. The PMBN/PLA nanoparticles could be prepared by the solvent evaporation technique. The initial concentration of PMBN was a very important factor to prepare the polymer nanoparticles. Table 2 shows the diameter and the surface ζ-potential of PMBN/PLA nanoparticles prepared by given concentrations of PMBN aqueous solution.

Table 1. Synthetic Result of PMBNs[a]

	mole fraction in feed			mole fraction in polymer					
abb.	MPC	BMA	MEONP	MPC	BMA	MEONP	yield (%)	time (h)	solubility in water
PMBN40	0.40	0.50	0.10	0.66	0.28	0.06	74	4	+
PMBN30	0.30	0.60	0.10	0.48	0.43	0.09	58	4	−
PMBN20	0.20	0.70	0.10	0.35	0.55	0.10	49	6	−

[a] [monomer] = 1.0 mol L⁻¹, [AIBN] = 10 mmol L⁻¹, temperature = 60 °C in ethanol. Determined by ^{1}H-NMR spectrum. Solubility was determined with 10 mg mL⁻¹ of each polymer sample and described as soluble (+) and insoluble (−) at 25 °C.

Table 2. Characterization of PMBN/PLA Nanoparticles Prepared with Various Concentrations of PMBN[a]

PMBN (mg/mL)	diameter (nm)	ζ-potential (mV)
10.0	195	−5.3
1.0	204	−6.2
0.1	627	−6.7

[a] Preparation condition: PLA concentration 10 mg/mL. ζ-potential measurement was carried out in 10 mM NaCl aq. solution.

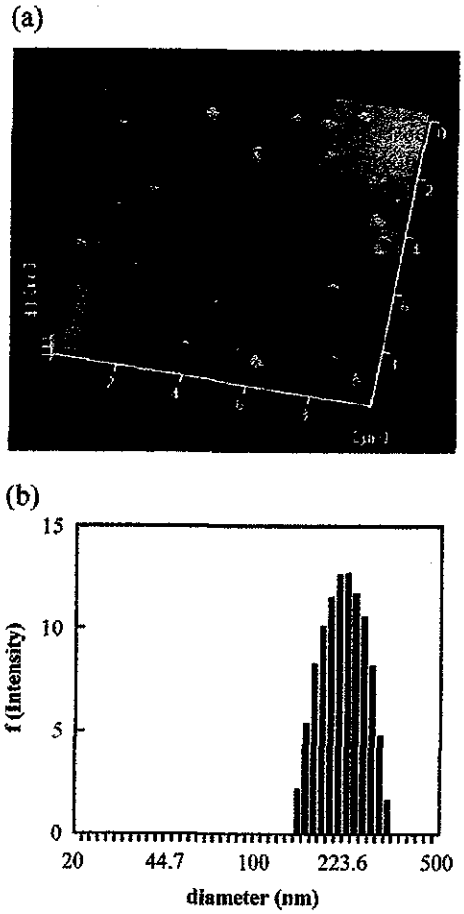

Figure 3. (a) AFM image of PMBN/PLA nanoparticles and (b) size distribution of PMBN/PLA nanoparticles prepared in 1.0 mg/mL PMBN.

The diameter of the PMBN/PLA nanoparticles was determined by DLS measurement. The diameter and ζ-potential was affected by the initial concentration of PMBN. When the initial concentration of PMBN was over the critical aggregate concentration from the fluorescence measurement of ANS (1.0 mg/mL), the diameter was 204 nm as the cumulant result in Marquadt analysis. In this case, the nanoparticles were stably dispersed in water. Figure 3 shows the AFM image (a) of the PMBN/PLA nanoparticles and the diameter histogram (b) from the DLS measurement.

This observation also indicated that the PMBN/PLA nanoparticles were spherical in shape and ca. 200 nm in diameter. The XPS charts of C1s, O1s, P2p, and N1s on the surface of the PMBN/PLA nanoparticles are shown in Figure 4. The PMBN/PLA nanoparticles had a phosphorus peak, a nitrogen peak, an oxygen peak, and a strong carbon peak

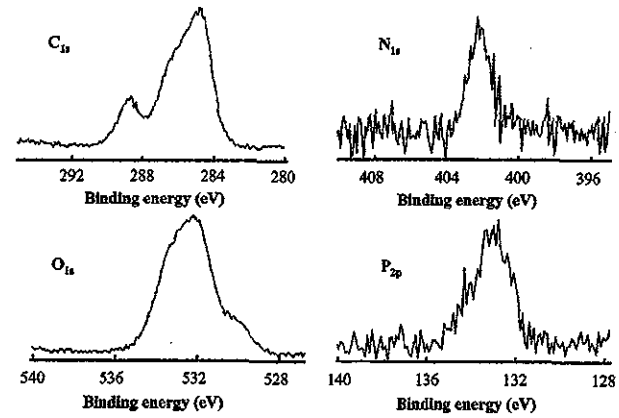

Figure 4. XPS charts of PMBN/PLA nanoparticles prepared in 1.0 mg/mL PMBN.

attributed to the methyl or methylene carbons. The surface of the PMBN/PLA nanoparticles was considered to be covered with phosphorylcholine groups in the MPC unit. Based on these results, it was indicated that the PMBN effectively acted as an emulsifier and a surface modifier due to its amphiphilic character.

To quantify the *p*-nitrophenyl ester groups on the nanoparticles, hydrolysis of the *p*-nitrophenyl ester bond in 0.01 M NaOH aqueous solution was carried out. The UV spectra of the *p*-nitrophenol released from the PMBN/PLA nanoparticles were detected, and the amount of active ester units on the PMBN/PLA nanoparticles was 7.6×10^{-9} mol/mg of nanoparticles.

An enzyme, ChO, was immobilized on the PMBN/PLA nanoparticles via condensation between the active ester groups and the amino groups of ChO. The immobilization reaction with the enzymes on the polymer nanoparticles induces release of *p*-nitrophenol with time. The obtained nanoparticles were called as ChO/PMBN/PLA nanoparticles. Un-conjugated ChO was removed completely from the nanoparticles by centrifugation. The schematic illustration of microdialysis sensor developed in this study was shown in Figure 5.

The obtained ChO/PMBN/PLA nanoparticles were filled into the microdialysis probe to create the enzymatic sensor. After addition of choline chloride as the substrate for ChO into the outer medium, the enzyme reaction occurred on the ChO/PMBN/PLA nanoparticles and produced hydrogen peroxide, which could be detected on the hydrogen peroxide electrode in the microdialysis probe [Figure 6a]. Figure 6b indicated an increase in current with the concentration of choline chloride in the outer solution. There was a good linear relationship between them; that is, the enzymatic reaction between immobilized ChO and the substrate choline chloride proceeded well.

Next, we carried out a dual-mode conjugation, which means immobilization of two kinds of enzymes on the same nanoparticle. As shown in Figure 7, when acetylcholine chloride was added in the outer solution, in which the microdialysis probe containing polymer nanoparticles was immersed, an increase in the current value could also be detected.

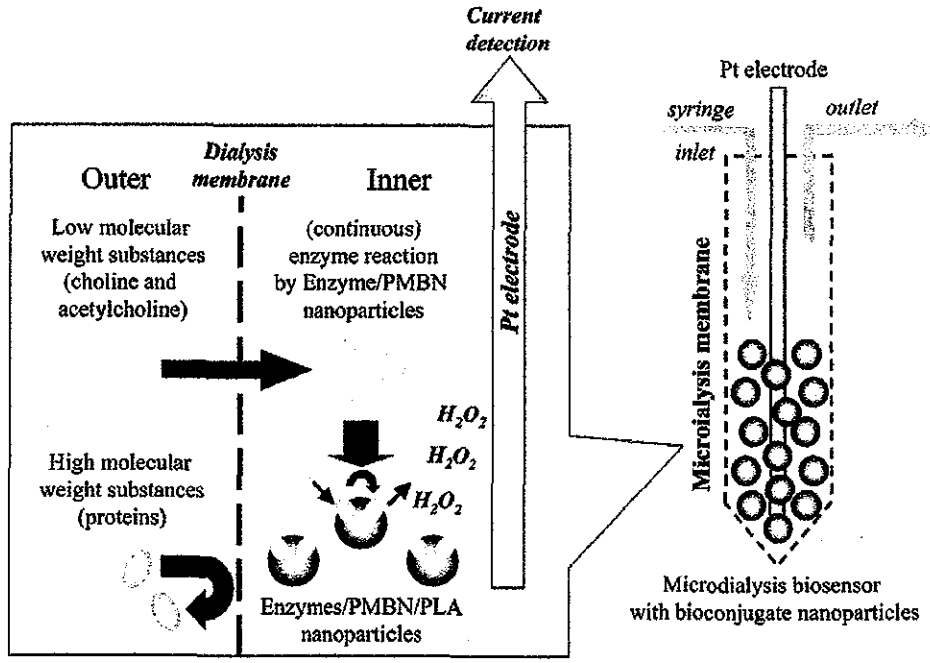

Figure 5. Schematic illustration of microdialysis biosensor system with bioconjugate nanoparticles.

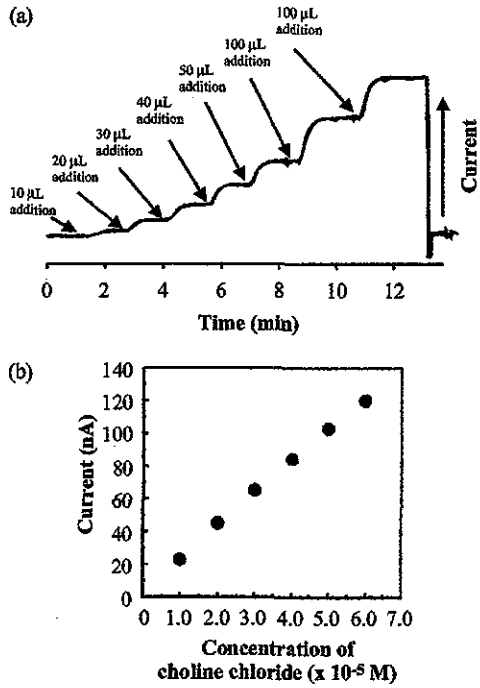

Figure 6. Enzymatic reaction of ChO on the surface of PMBN/PLA nanoparticles in the microdialysis probe, (a) the relationship between the change in the current value and the measurement time (outer medium was 50 mL; concentration of added choline chloride 1.5 mg/mL) and (b) the relationship between the concentration of added choline chloride and the current value.

Namely, the continuous enzymatic reaction could occur on the surface of polymer nanoparticles. As in the case of dual-mode conjugation of two kinds of enzymes, the local concentration of enzymes was higher, that is, the distance between AChE and ChO was small. Diffusion of the first product (choline) with AChE was easier and the choline was reacted with the second enzyme, ChO, as a second substrate. Therefore, the continuous enzyme reaction could occur smoothly. Based on these results, it was considered that the polymer nanoparticles could conjugate with specific biomolecules and these bioconjugated nanoparticles could be used in a diagnostic system. ACh is one of the most important neurotransmitters and is also believed to be involved in some severe diseases such as Alzheimer's, Parkinson's, epilepsy, and so on.[12,13] However, a real-time monitoring using a microdialysis system is difficult because the flow rate of the perfusion solution is quite slow. Therefore, the microdialysis system needs a long time to collect the analyte samples.[14,15] In this study, we confirmed that the continuous enzyme reactions occurred by dual-mode conjugation of two kinds of enzymes (ChO and AChE) on the polymer nanoparticles. From these findings, a novel diagnostic system can be prepared using the bioconjugated polymer nanoparticles covered with phosphorylcholine groups in the microdialysis probe.

Conclusion

A novel MPC polymer having *p*-nitrophenyl ester groups was designed and synthesized in this study. The MPC polymer had an amphiphilic character, and it could be used as an emulsifier and surface modifier for preparing polymer nanoparticles covered with phosphorylcholine groups and active ester groups. Two kinds of enzymes could be immobilized on the surface of the nanoparticles, and they could perform their specific function in the microdialysis probe. Continuous enzymatic reactions were realized on the polymer nanoparticles. That is, one substrate was added in the outer solution of the microdialysis probe containing polymer nanoparticles; it permeated through the hollow fiber and reacted with one enzyme on the polymer nanoparticles.